Matrix Metalloproteinase Target Family Landscape: A Chemometrical Approach to Ligand Selectivity Based on Protein Binding Site Analysis

Bernard Pirard* and Hans Matter

Science and Medical Affairs, Chemical Sciences, Drug Design, Aventis Pharma Deutschland GmbH, a Company of the Sanofi-Aventis Group, D-65926 Frankfurt am Main, Germany

To gain insight into the structural determinants for the matrix metalloproteinase (MMP) family, we characterized the binding sites of 56 MMP structures and one TACE (tumor necrosis factor α converting enzyme) structure using molecular interaction fields (MIFs). These MIFs were produced by two approaches: the GRID force field and the knowledge-based potential DrugScore. The subsequent statistical analysis using consensus principal component analysis (CPCA) for the entire binding site and each subpockets revealed both approaches to encode similar information about discriminating regions. However, the relative importance of the probes varied between both approaches. The CPCA models provided the following ranking of the six subpockets based on the opportunity for selective interactions with different MMPs: S1′ > S2, S3, S3′ > S1, S2′. The interpretation of these models agreed with experimental binding modes inferred from crystal structures or docking.

1. Introduction

Together with combinatorial chemistry, high-throughput screening (HTS) was expected to deliver many new lead compounds for the pharmaceutical industry. However, after a few years, the limitations of HTS have led to a paradigm shift toward knowledge-driven approaches to lead discovery such as virtual screening[1−3] and structure-based design.[4−8] Because the completion of the human genome has posed new challenges to the pharmaceutical industry, novel technologies and parallelization have accelerated aspects of the research process. However, exploiting knowledge of particular protein target families is expected to revolutionize the drug discovery process. Major protein familes, as defined by the protein sequence and structural homology level, include kinases, proteases, G-protein-coupled receptors, ion channels, and others. The strategy based on protein target families is often referred to as the *chemical biology*[9−11] approach. Typical targets within a protein family often share similar in vitro assays and properties.[11] Hence, it could be expected that a significant percentage of molecules designed to interact with a particular member of one family will also show some activity against other family members. These other family members might be involved in a different biological function.[12] Chemical biology entails the identification of structural features or motifs that determine ligand binding to a particular protein target family. These motifs can be subsequently incorporated in target family-focused chemical libraries.[13,14] A detailed understanding of structural parameters determining selectivity is another prerequisite for target family-based approaches. Those discriminating features have to be built in novel scaffolds to yield high-quality lead compounds.

The exponentially growing number of protein three-dimensional (3D) structures[15] provides an invaluable source of detailed information about target families, which could be combined with ligand-derived knowledge. Typically, 3D structures for a target family can be aligned in a common reference frame for a comparative analysis. This allows for identifying favorable protein−ligand interactions in different binding sites using force field or knowledge-based approaches such as the program GRID[16,17] and others. However, this produces many data points to enable visual inspection of common interaction patterns. Therefore, chemometrical tools such as principal component analysis (PCA[18]) are utilized for extracting relevant information from those molecular interaction field (MIF) maps. Principal component analysis on multivariate GRID descriptors was previously applied to uncover differences between two binding sites with respect to their probe interaction patterns for targets such as DNA,[19] dihydrofolate reductase,[20] matrix metalloproteinases,[21,22] and cyclooxygenase.[23] However, the original formulation of the GRID/PCA approach had some drawbacks. These include difficulty understanding the relative importance of individual probes for selectivity and its limitation to pairs of targets. This latter makes the interpretation difficult for analyses involving multiple targets. Hence, an improved formulation, called GRID/consensus PCA (GRID/CPCA[24,25]) was developed to compare the binding sites of representative members of the serine protease,[24,26] cytochrome P450 2C,[27] and kinase families,[28] to name a few applications. Those consensus multivariate analysis tools such as CPCA eliminate the block-scaling problem and the need for variable deletion and greatly simplify the chemical interpretation. The GRID/CPCA derived score plots reveal the grouping of target family members by structural similarities within their binding sites. The loading plots highlight those regions of the common binding sites of a protein family, where selective interactions with a given probe could be obtained for only a few members. As a result, the biological space of a protein target family is defined in 3D structural terms, named "target family landscape".[28]

In this paper, we describe the target family landscape for the protein family of matrix metalloproteinases (MMPs). This study provides an extension to the MMP selectivity problem from analyzing only two family members, namely, MMP-3 and MMP-8.[21,22] Terp and colleagues[29] also applied GRI/CPCA to 10 MMPs including 5 MMP X-ray structures and 5 homology models (for MMP-9, -12, -13, -14, -20). In addition to expected differences in the S1′ pocket, the importance of the unprimed

---

* To whom correspondence should be addressed. Present address: Novartis Institute for BioMedical Research, WSJ507.1.51, CH-4002 Basel, Switzerland. Phone: ++41-61-32-45620. Fax: ++41-61-69 68 676. E-mail: bernard.pirard@novartis.com.

Table 1. Summary of MMP and TACE Catalytic Domain X-ray Crystal Structures Retrieved from ReliBase+ Plus Homology Models Used for This Study

| metalloproteinase subfamily	color	type	PDB code/homology model
collagenases	red	MMP-1	1CGE, 1CGF, 1CGL, 1FBL, 1HFC, 2TCL, 966C
		MMP-8	1A85, 1A86, 1BZS,[a] 1JAN, 1JAO, 1JAP, 1JAQ, 1JJ9, 1KBC, 1I73, 1I76, 1MMB, 1MNC
		MMP-13	1CXV, 456C, 830C
gelatinases	cyan	MMP-2	1CK7,[b] 1QIB
		MMP-9	homology model
stromelysins	green	MMP-3	1BIW, 1BQO, 1B3D, 1B8Y, 1CAQ, 1CIZ, 1CQR, 1C3I, 1C8T, 1D5J, 1D7X, 1D8F, 1D8M, 1G05, 1G4K, 1G49, 1HFS, 1SLM, 1SLN, 1UEA, 1USN, 2USN
		MMP-10	homology model
		MMP-11	1HV5
matrilysin	orange	MMP-7	1MMP, 1MMQ, 1MMR
macrophage metalloelastase	magenta	MMP-12	1JK3
membrane type MMP	blue	MMP-14	1BQQ, 1BUV
		MMP-16	homology model
TACE	yellow		1BKC

[a] MMP-8 template catalytic domain for structure alignment (resolution 1.7 Å). [b] Rejected for final analysis, as full length X-ray crystal structure with sterically hindered active site.

MMP subsites S3 and S2 for selective inhibition was highlighted.[30,31] These results suggested the possibility of discriminating between 8 of the 10 MMPs. Another approach compared the structures of 24 MMPs (9 X-ray, 15 homology models) in terms of force field interaction energies and ranked MMP subsite similarities on that basis in decreasing order as follows: S1′ (most similar) > S2 > S3′ > S1 ∼ S3 > S2′ (less similar).[32]

The present study is based on 57 protein structures including 54 X-ray structures of 10 different members of the MMP family plus three homology models for MMP-9, -10, and -16, respectively (Table 1). This adds a lot of novel experimental information plus conformational diversity to this selectivity analysis. Furthermore, a large set of MMP selective ligands is compared to these CPCA models for different subpockets. Finally, we have explored the replacement of the GRID force field by knowledge-based potentials to characterize favorable protein−ligand interactions using the program DrugScore.[33,34] This should allow a general description of selectivity differences using an independent approach based on statistical analysis of experimental data. Consistently these additions provide more insight into essential prerequisites for ligand selectivity.

DrugScore had been derived earlier using structural information from 1376 crystallographic ligand−protein complexes.[35,36] This information was converted into distance-dependent pair preferences and solvent-dependent singlet preferences for ligand and protein atoms.[33] Similar approaches for scoring protein−ligand interactions and ranking binding poses have emerged,[37] like PMF[38] and BLEEP.[39] Applications of DrugScore include the recognition of near native binding modes from flexible docking,[33] the prediction of binding affinities,[33,34] its use as an objective function in docking,[40] and identification of hot spots in binding cavities.[34] In this case, regions of high binding propensities for defined atom types are displayed as isosurfaces.[34] These hot spots are computed on the basis of a regularly spaced grid inside the binding site; scoring values are calculated at every point using different atom types. From analysis of 158 protein−ligand complexes, the spatial coincidence of hot spots with experimentally observed similar ligand atoms was found between 74% and 85% depending on the atom classification.[40] This knowledge-based potential is fast to compute and robust. Because only non-hydrogen atoms are considered to derive the pair potentials, it does not require any assumptions on protonation states.

The MMPs are calcium- and zinc-dependent endopeptidases involved in the degradation of the extracellular matrix and tissue remodeling.[41,42] Selective MMP inhibitors, being explored as new therapeutic targets in several pharmaceutical companies, may have value in diseases such as cancer, arthritis, and cardiovascular diseases.[41,43] Currently, at least 21 mammalian MMPs have been discovered, including three collagenases (MMP-1, -8, and -13), two gelatinases (MMP-2 and MMP-9), three stromelysins (MMP-3, -10, and -11), one matrilysin (MMP-7), one macrophage metalloelastase (MMP-12), and five membrane type MMPs (MMP-14 through MMP-17 and MMP-24). Under normal physiological conditions, their activity is tightly controlled through transcriptional regulations by cytokines and growth factors, secretion as inactive proenzymes, requiring specific activation, and the presence of endogenous tissue inhibitors of MMPs.[44] Misregulation of MMPs leads to an excessive degradation of the extracellular matrix and is believed to contribute to pathological conditions such as cancer,[45] angiogenesis, osteoarthritis,[46] rheumatoid arthritis,[47] remodeling in Alzheimer disease,[48] and pulmonary emphysema.[43] Most members of the MMP family share the same organization into three basic, distinct, and well-conserved domains, namely, an amino terminal propeptide, a catalytic domain, and a hemopexin-like domain at the carboxy terminal.[41,49−51] So far, the catalytic domain has been the target of many medicinal chemistry efforts aiming at the treatment of the above-mentioned diseases. Over the past couple of years, both crystal and solution structures of several ligand-free and ligand-bound MMPs have been described.[52] All structures exhibit the characteristic fold of zinc-dependent endopeptidases consisting of a five-stranded β sheet and three helices (Figure 1A). Furthermore, the X-ray structure of activated full length MMP-1[53] reveals that the architecture of the active site in the isolated catalytic domain is maintained in the full-length protein. These structural analyses have also confirmed the biochemical results that six subsites, three on either side of the cleavage site, are mandatory for the observed proteolytic activity. Because the available 3D structures provide some insight into the structural determinants of selectivity, this study aims to identify combinations of interactions that would allow inhibiting a particular MMP while sparing the others.
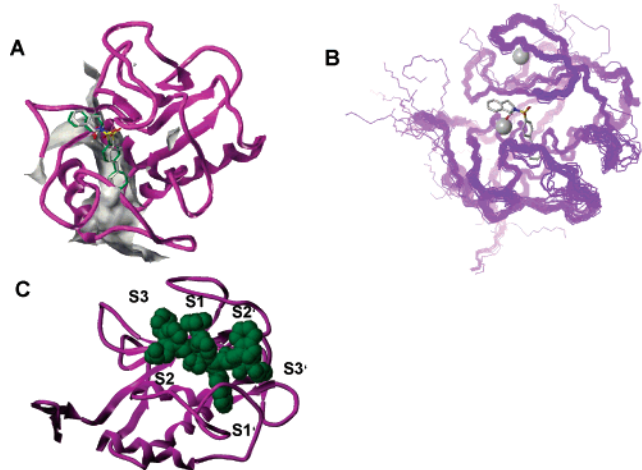
Figure 1. (A) Characteristic fold of the catalytic domain for Zn-dependent endopeptidases indicated by a ribbon-tube encoding secondary structural elements for the 1.7 Å X-ray structure of human neutrophil collagenase (MMP-8) in complex with compound **4** (PDB code 1BZS, Chart 1). The inhibitor binding site is highlighted by a GRID interaction energy contour map based on a methyl probe, drawn at +1 kcal/mol. Depth cueing is used to allow for a view into the S1′ pocket, where the biphenyl substituent is located. (B) Alignment of 53 X-ray structures and three homology models for the MMP target family using the alignment approach described in the text considering the crystal structure of compound **4** bound to MMP-8 (PDB code 1BZS) as reference. Both Zn ions are shown as white spheres. Compound **4** from the template MMP structure is also displayed. (C) Six subpockets of the MMP binding site displayed as space filling models of compounds **5** and **7** and a tripeptide bound respectively to MMP-3, -11, and 08 (PDB codes 1BIW, 1HV5, and 1JAP). The structure of MMP-11 (PDB code 1HV5) is shown as reference.

2. Results and Discussion

2.1. Classification of MMPs and TACE Using GRID/DrugScore PCA.
As the first step, the GRID and Drug-Score derived interaction fields were analyzed for the aligned protein structures (Figure 1B) using PCA. This analysis yielded a global classification of the MMP structural family, which we refer to as "target family landscape".[28] The score plots summarizing 3D binding site similarities among MMPs are given in Figure 2 for GRID and DrugScore interactions, respectively.

For the GRID derived PCA model (Figure 2A), the first principal component (PC1) discriminates the following MMPs: MMP-8 (negative PC1) from two stromelysins (MMP-3, -10) with positive PC1 score; MMP-1 (negative PC1) from MMP-7 (positive PC1). Most of the remaining MMPs (MMP-2, -9, -11, -12, -13, and -14) are located in the region between the MMP-8 and the MMP-3 ensembles. Interestingly, the third stromelysin (MMP-11) is more related in terms of favorable binding site interactions to MMP-8 and -12 than to the other two stromelysins MMP-3 and -10. This agrees with results of multiple sequence alignment and clustering studies.[54] These revealed a similarity between MMP-3 and -10, while MMP-11 is clearly separated.

The second principal component (PC2) separates nearly all of the MMP-1 and MMP-7 from most of the other MMPs. It is also noteworthy that MMP-1 and -3 structures are spread over two and three clusters, respectively. These clusters could be related to conformational flexibility, in particular MMP sub-pockets, as discussed below.

Adding the less similar metalloproteinase TACE (tumor necrosis factor α converting enzyme) to this target family
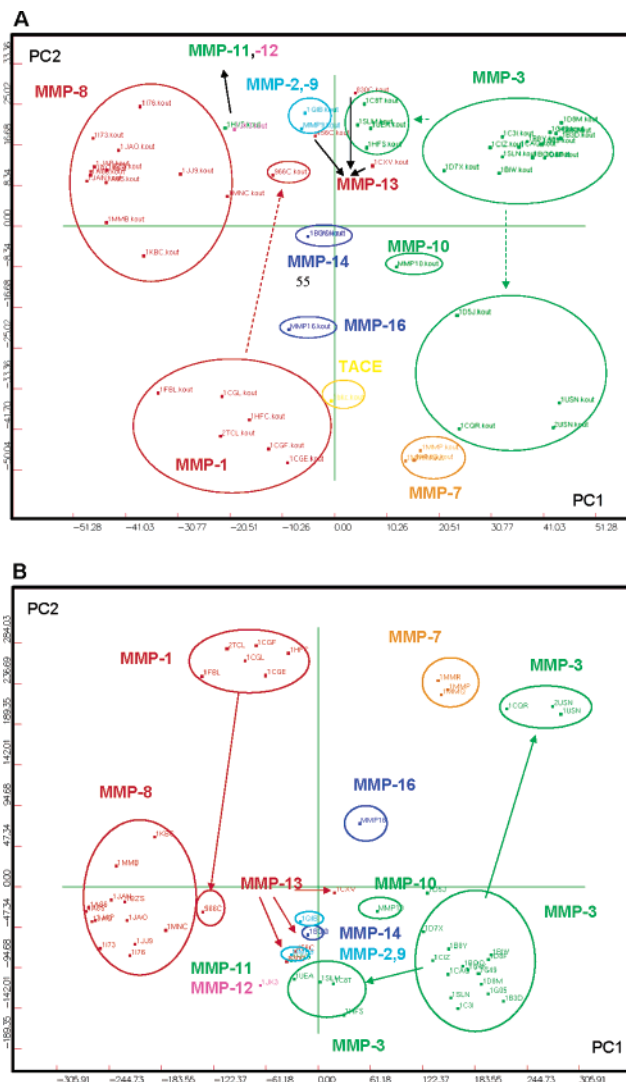

Figure 2. MMP target family landscape based on GRID/PCA and DrugScore/PCA score plots for the superimposed metalloproteinases: (A) PCA using GRID descriptors for 56 MMPs plus TACE; (B) PCA using DrugScore descriptors for 56 MMP structures. The color code for particular metalloproteinase subfamilies is according to Table 1.

landscape does not change the original PCA score plot. Hence, only this PCA map is shown in Figure 2A. The TACE structure is located in a region close to MMP-1 and MMP-16, which implies similar ligand recognition motifs and structure–activity relationship homology[55] for these metalloproteinases. This classification of MMPs is based only on favorable protein–ligand interactions of their ligand binding sites without considering sequence similarity or ligand structure.

Replacing the GRID force field descriptors by DrugScore derived knowledge-based potentials only slightly affects the positions of individual clusters on the PCA map, while no changes in the relationship of individual clusters are found (Figure 2B). The major difference is the sign inversion for the second PC, causing the ensemble of MMP-1 and -7 to be located in the upper moiety of this map. All other features are similar, suggesting a significant relationship between individual MMPs on the basis of their potential protein–ligand interactions. This seems to be consistently treated in both the GRID force fields and the DrugScore knowledge-based approach. The following sections will focus on selectivity results and chemical interpreta-
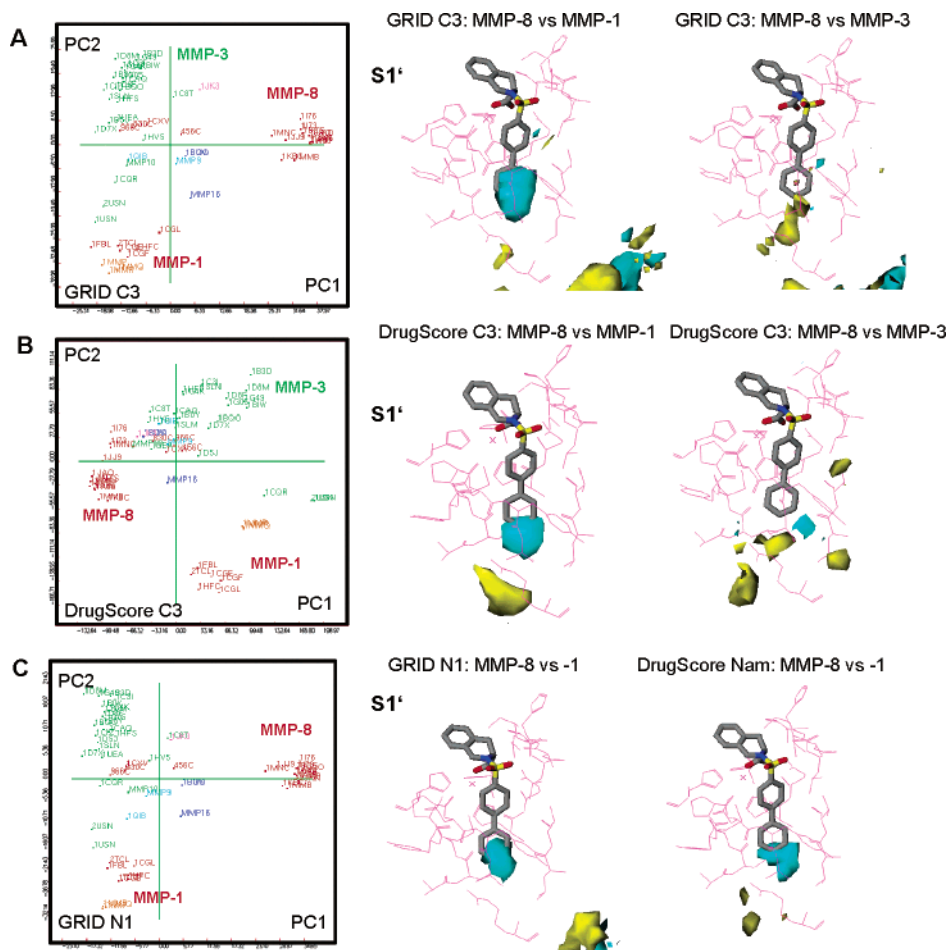
Figure 3. (Continued on next page)

tion of GRID and DrugScore CPCA models for individual MMP subsites (Figure 1C).

2.2. Focused GRID/DrugScore CPCA Analysis of MMP Subpockets: S1′. The S1′ site, also called specificity pocket, is the most prominent pocket within the MMP catalytic domain. This pocket is characterized by two main features: the residue at position 218 (MMP-8 numbering)[56,57] and a loop at the back of this pocket. Sequence alignments and X-ray crystal structures show that this pocket is surrounded by a loop with variable-length amino acid composition and conformation in different family members. Hence, it is assumed that a 3D binding site derived analysis provides a deeper level of detail on favorable interactions required for a particular selectivity profile in MMPs. Differences in the size and shape of this pocket suggest that this pocket critically determines MMP selectivity.[21,22,29] The importance of filling the S1′ pocket by adequate chemical functionalities has been previously discussed.[21,58] The findings and structural implications for selectivity from the present analysis are summarized below.

The most important GRID probes for discrimination between individual members of the MMP family with respect to the S1′ pocket are methyl (C3), amide nitrogen (N1), and carbonyl oxygen (O), as revealed by inspecting the CPCA superweights. These superweights indicate the contribution of each individual CPCA submodel to the final CPCA model. For DrugScore, this analysis highlights particularly the C.3, C.2, and Cl probes as relevant for discrimination. Selected CPCA submodels are displayed in Figure 3 on the left for the GRID C3 (A), N1 (C), and O (D) probes as well as for the DrugScore C.3 atom type (B). The MMP discrimination from the GRID methyl probe

(Figure 3A) and the DrugScore C.3 atom type (B) are qualitatively similar. They only differ in the sign of the PC1 axis, suggesting a similar interpretation in structural terms from both complementary descriptor approaches to protein selectivity. In both, the MMP structures are colored by subfamilies according to the scheme provided in Table 1.

In the GRID and DrugScore derived PCA and all CPCA block models focused on the S1′ pocket, except for the DRY probe, PC1 separates the MMP-3 S1′ pocket on the left with negative scores from the cluster of MMP-8 structures on the right with positive scores. For DrugScore, the MMP-3 S1′ pocket is consistently located on the right of PC1. The second PC for both GRID and DrugScore discriminates the ensembles of experimental MMP-1 and MMP-7 structures from MMP-3. This difference agrees with the observation of two distinct types of S1′ specificity pockets in MMPs:[57] a large, open pocket type as observed, for example, in structures of MMP-3, -8, and -13 and a small, closed pocket, exemplified in MMP-1 (not all known X-ray structures) and MMP-7 (matrilysin).[59] All other MMPs occupy a region included in the triangle defined by the MMP-1, -3, and -8 clusters.

A large cluster plus a singleton structure (PDB code 966C) represents the conformationally diverse MMP-1 enzyme. The latter structure differs from the larger MMP-1 cluster by the conformational state within the S1′ pocket. This S1′ pocket within the human fibroblast collagenase MMP-1 is able to undergo a conformational change in multiple side chains upon inhibitor binding; e.g., Leu181, Arg214, Val215, Ser239, Tyr240, Phe242 can adopt an open conformation for binding a ligand with a large S1′ directed diphenyl ether moiety, like
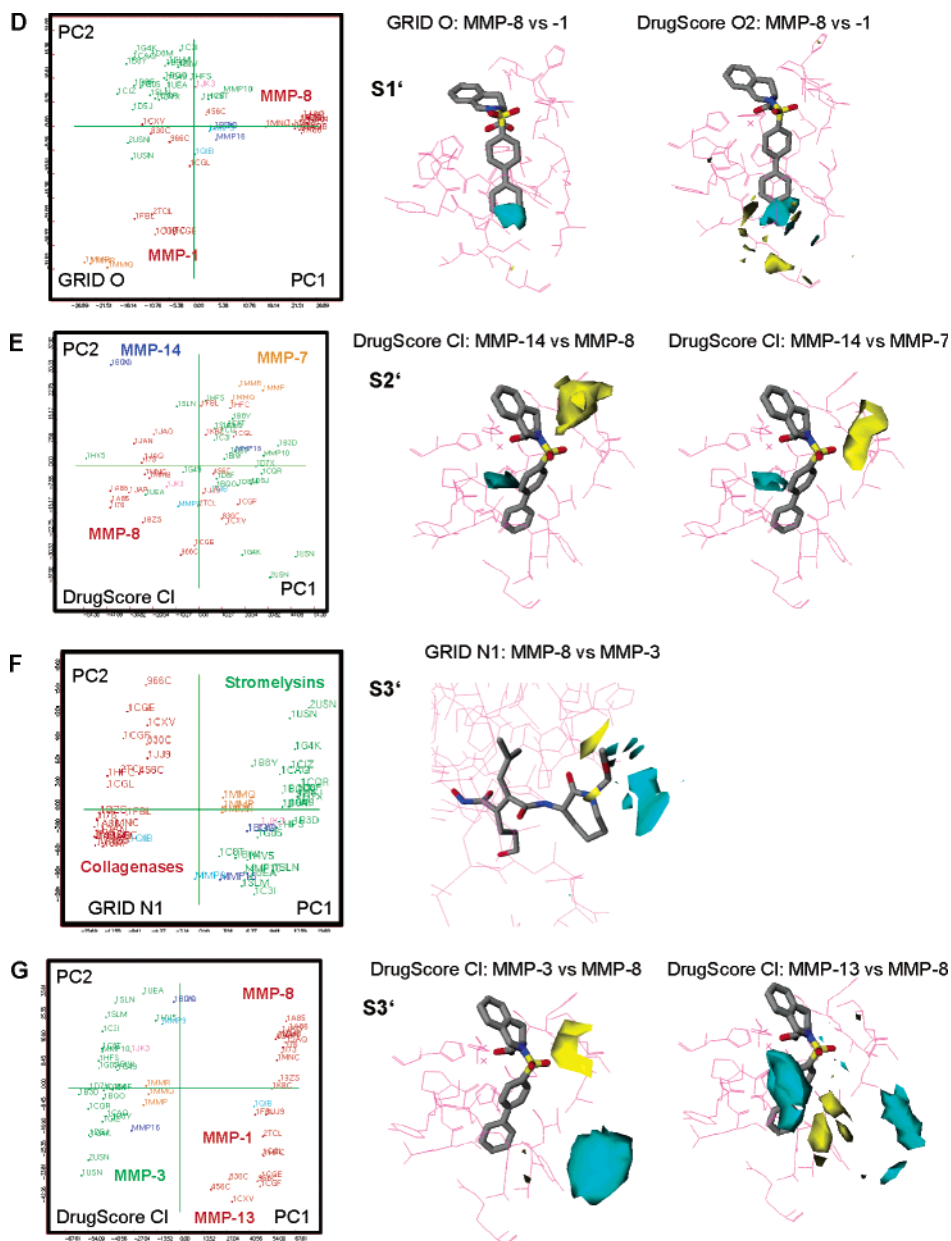
Figure 3. CPCA submodels for MMP prime pockets (S1′ (A−D), S2′ (E), S3′ (F, G)) obtained from GRID and DrugScore. Middle and right panels highlight regions of the prime pockets where selectivity between different MMPs can be gained using a given probe. Compound **4** (Chart 1) bound to MMP-8 (PDB code 1BZS) is displayed as reference for all the prime pockets, except S3′, where compound **5** (Chart 1) bound to MMP-3 (PDB code 1BIW) is shown as reference. (A) CPCA score plot of S1′ for the GRID C3 probe (left panel); favorable interactions to discriminate the S1′ pockets of MMP-8 (PDB code 1BZS, cyan) and MMP-1 (PDB code 1CGE, yellow) using the GRID C3 probe (middle panel); favorable interactions to discriminate the S1′ pockets of MMP-8 (PDB code 1BZS, cyan) and MMP-3 (PDB code 1BIW, yellow) using the GRID C3 probe (right panel). (B) CPCA score plot for the DrugScore C.3 probe (left panel); favorable interactions to discriminate the S1′ pocket of MMP-8 (PDB code 1BZS, cyan) and MMP-1 (PDB code 1CGE, yellow) using the C3 probe (middle panel); favorable interactions to discriminate the S1′ pocket of MMP-8 (PDB code 1BZS, cyan) and MMP-3 (PDB code 1BIW, yellow) using the C3 probe (right panel). (C) CPCA score plot for the GRID N1 probe (left panel); favorable interactions to discriminate the S1′ pocket of MMP-8 (PDB code 1BZS, cyan) and MMP-1 (PDB code 1CGE, yellow) using the GRID N1 (middle panel) and DrugScore N.am probes (right panel). (D) CPCA score plot for the GRID O probe (left panel); favorable interactions to discriminate the S1′ pocket of MMP-8 (PDB code 1BZS, cyan) and MMP-1 (PDB code 1CGE, yellow) using the GRID O (middle panel) and DrugScore O.2 probes (right panel). (E) CPCA score plot for the DrugScore Cl probe (left panel); favorable interactions to discriminate the S2′ pocket of MMP-14 (PDB code 1BQQ, yellow) and MMP-8 (PDB code 1BZS, cyan) using the DrugScore Cl probe (middle panel); favorable interactions to discriminate the S2′ pocket of MMP-14 (PDB code 1BQQ, cyan) and MMP-7 (PDB code 1MMP, yellow) using the DrugScore Cl probe (right panel). (F) CPCA score plot for the GRID N1 probe (left panel); favorable interactions to discriminate between MMP-8 (PDB code 1BZS, cyan) and MMP-3 (PDB code 1BIW, yellow) using the GRID N1 probe (right panel). (G) CPCA score plot for the DrugScore Cl probe (left panel); favorable interactions to discriminate the S3′ pocket of MMP-3 (PDB code 1BIW, cyan) and MMP-8 (PDB code 1BZS, yellow) using the DrugScore Cl probe (middle panel); favorable interactions to discriminate the S3′ pocket of MMP-13 (PDB code 830C, cyan) and MMP-8 (PDB code 1BZS, yellow) using the DrugScore Cl probe (right panel).

compound **1** (Chart 1).[60−62] The presence of this large substituent requires Arg214 to adopt a new position, which enlarges the MMP-1 S1′ pocket. The observed selectivity for the diphenyl

ether series toward MMP-13 (collagenase-3) is largely determined by the affinity toward the preformed S1′ pocket, compared to the induced fit in MMP-1, which might be

Chart 1
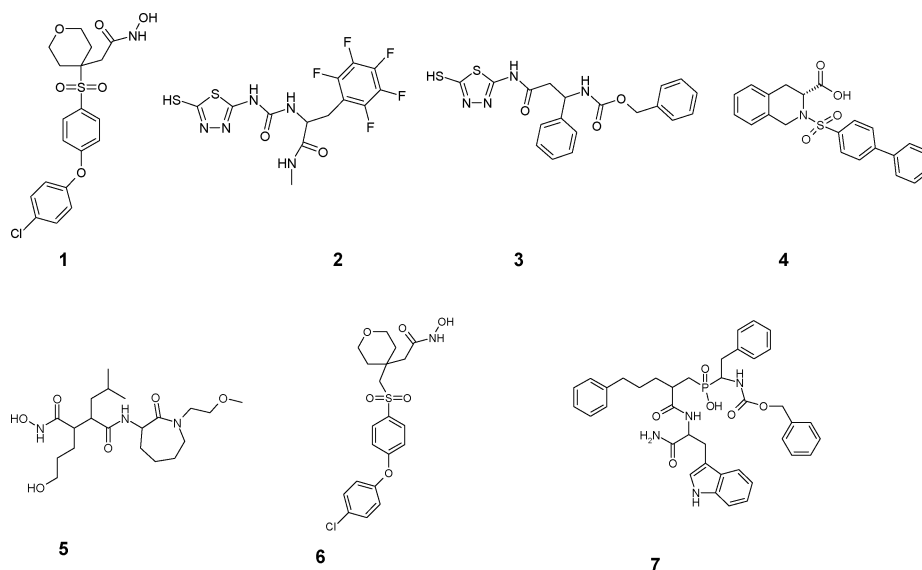
energetically less favored for binding. This is reflected by selectivity ratios of 177−1135 for MMP-13 vs MMP-1 in related derivatives.[60]

The stromelysin-1 (MMP-3) structures are distributed over three clusters: a large cluster containing 18 of the 22 MMP-3 structures, a smaller cluster populated by one apo form (PDB code 1CQR) plus two structures crystallized with compounds **2** and **3** (Chart 1) that do not bind to the S1′ subpocket (PDB codes 1USN and 2USN),[31] and a singleton (PDB code 1C8T[63]). For this latter structure, the region encompassing Leu229-Thr-Arg-Phe-Arg233 of the loop at the bottom of the S1′ pocket exhibits a different conformation compared to those structures within the larger MMP-3 cluster. For two MMP structures (PDB codes 1C8T and 1CAQ), the centers of the Arg233 side chain are 4.0 Å from each other, affecting the accessibility of the S1′ pocket. Despite these local conformational differences, the protein backbone atoms surrounding the S1′ pocket are well aligned, as illustrated by a root-mean-squared (rms) standard deviation of 1.71 Å for two MMP-3 structures found in two different clusters (PDB codes 1C8T and 1B3D).

The MMP subfamily selectivity differences are plotted in Figure 3 as CPCA differential plots for the GRID C3 (A), N1 (C), and O (D) probes plus the DrugScore C.3 atom type (B). These exhibit strong contributions to both PC1 and PC2 in the corresponding CPCA analyses. Cyan contour regions in Figure 3 indicate protein−ligand interactions for that particular probe favorable for MMP-8, while yellow contours highlight favorable interactions with MMP-1 (middle panel) or MMP-3 (right panel) only, as obtained using GOLPE pseudofield plots.[64] The crystal structure of compound **4** (Chart 1) bound to MMP-8 (PDB code 1BZS[58]) is displayed for comparison. Discriminations along PC1 (e.g., separating MMP-3 and MMP-8) are determined by structural differences at the bottom of the S1′ pocket, namely, in the specificity loop. In PC2, positive interactions (yellow) characterize favorable interactions for MMP-3 and its neighbors, while negative regions (cyan) are favorable for MMP-1 and the neighboring proteins. In contrast, the separation along PC2 (e.g., MMP-8 versus MMP-1) is mainly driven by changes at a single position, namely, 197 (MMP-3 numbering). This is consistent among different methods (DrugScore or GRID) and corresponds to previous findings.[29]

A careful inspection of CPCA S1′ submodels also suggests opportunities to achieve selective interactions to other MMPs,

e.g., the membrane type MMP-16 and MMP-12. For example, the polar amide nitrogen N.am submodel indicates a discrimination of MMP-12 on the basis of favorable interactions with Thr215 (MMP-12 numbering). This amino acid at the wall of S1′ is replaced by valine in most of the other MMPs (e.g., Val198 in MMP-3) except for MMP-7 (Ala). This finding is also in agreement with another recent MMP-12 X-ray structure.[65]

2.3. Focused GRID/DrugScore CPCA Analysis of MMP Subpockets: S2′. The S2′ subsite is a shallow, solvent-exposed cleft whose surface is defined by the side chains of residues 158 and 159 (MMP-8 numbering) along the "top" face and by the side chain of residue 218 on the "bottom" face. The nature of protein−ligand interactions is determined by the amino acid in position 159 (MMP-8 numbering, e.g., Asn/MMP-1, Val/MMP-3, Thr/MMP-7, Ile/MMP-8, Phe/MMP-14) in combination with the solvent exposed side chain at the bottom position 218 for this pocket (Ser/MMP-1, Leu/MMP-3, Thr/MMP-7, Asn/MMP-8, Phe/MMP-11, -14, -15, -16). These amino acid differences correspond to the main favorable interaction differences after inspecting the GRID and DrugScore CPCA plots.

The most important DrugScore probes for separating MMP family members with respect to S2′ are chlorine (Cl), amide nitrogen (N.am), and sp[2] carbon (C.2). The CPCA submodel for the DrugScore Cl probe is shown in Figure 3E with MMPs colored by subfamilies according to Table 1. Favorable contours referring to individual members of this family are indicated in Figure 3E using compound **4** (Chart 1) bound to MMP-8 (PDB code 1BZS) as reference. This hydrophobic chlorine separates MMP-14 (blue) from other MMPs, mainly based on favorable interactions with the MMP-14 residue Phe198 (MMP-14 numbering). The corresponding favorable interaction with this residue is highlighted using a yellow contour region in Figure 3E, middle panel. This residue Phe198 is replaced by Ile159 in MMP-8 and by the more polar Thr180 in MMP-7. Obviously the interaction between chlorine and an aliphatic lipophilic side chain is weaker as for an aromatic ring. This interaction also discriminates between MMPs with polar residues at this position, as obvious from inspection of the CPCA score plot for this probe (Figure 3E, right panel). Again, interactions favoring MMP-14 binding are highlighted by yellow contours, while cyan interactions with the "bottom" residue of S2′ are favorable for MMP-8 and -7. It should also be mentioned that the GRID hydrophobic

probe (DRY) does not discriminate between MMP-14 and other MMPs. This observation suggests that the DrugScore Cl probe encodes more than hydrophobic interactions. Our analysis of the DrugScore Cl probe is consistent with the recently described interactions between Cl atoms and aromatic amino acids in protein−ligand complexes.[66] It is also noteworthy that the GRID Cl probe is also likely to produce results qualitatively similar to those of the DrugScore Cl probe.

The analysis of packing interactions of representative MMP protein−ligand complexes using ReliBase+[67] reveals for the majority of entries the influence of crystallographically related molecules especially in the S2′ binding site region. For example, this was observed for one MMP-1 structure (PDB code 2TCL[68,41]) and might produce unrealistic inhibitor conformations stabilized at the interface of this MMP dimmer. This does not necessarily represent the physiologically active state in solution. In contrast, the CPCA analyses were based on monomeric MMP structures to identify favorable interaction regions.

All these observations collectively make the S2′ site less valuable to achieve selective interactions. This conclusion agrees with our GRID/CPCA analysis, which shows a poor separation of the MMP subfamilies in the different CPCA scores plots.

2.4. Focused GRID/DrugScore CPCA Analysis of MMP Subpockets: S3′. The subsite S3′ is located at the edge of the MMP active site. Hence, any inhibitor binding to this subpocket is solvent-exposed and might also interact with crystallographically related MMP molecules, as discussed for S2′. In the full-length protein, the substrate-binding domain, coupled via a flexible linker to the catalytic domain, might be able to influence binding properties here. For all MMPs, except the stromelysin family, there is only little gain in inhibitor affinity on interaction with S3′. The stromelysins MMP-3 and -10 plus matrilysin MMP-7 are characterized by a polar amino acid at position 162 (MMP-3 numbering, Asn162 in MMP-3 and -7, His162 in MMP-10), while Gly is present in all other proteins including the stromelysin MMP-11. Hence, favorable interactions with carbonyl oxygen probes are observed for those proteins with polar residues in this region. The size and polarity of this pocket are also determined by the amino acid at position 193 (Thr for stromelysins and MMP-12, Ile for MMP-7, Asn for MMP-14 and -16, Gln for MMP-9, and Tyr for the remaining MMPs).

The most important GRID probes for separating the MMP family members with respect to S3′ are N1, OH, O, and C3. The first PC in the PCA and all the individual CPCA block models but the DRY one separate an extended cluster containing the collagenases (MMP-1, -8, -13) plus MMP-2 on the left with negative PC1 scores for GRID/CPCA or positive scores for DrugScore/CPCA from another extended cluster on the opposite side populated by all stromelysins (MMP-3, -10, -11), MMP-7, MMP-9, MMP-12, the membrane type MMPs (MMP-14 and -16), and TACE (Figure 3F−G). On the other hand, the second PC cannot discriminate between the different MMP subfamilies, while individual differences within each subfamily can be detected.
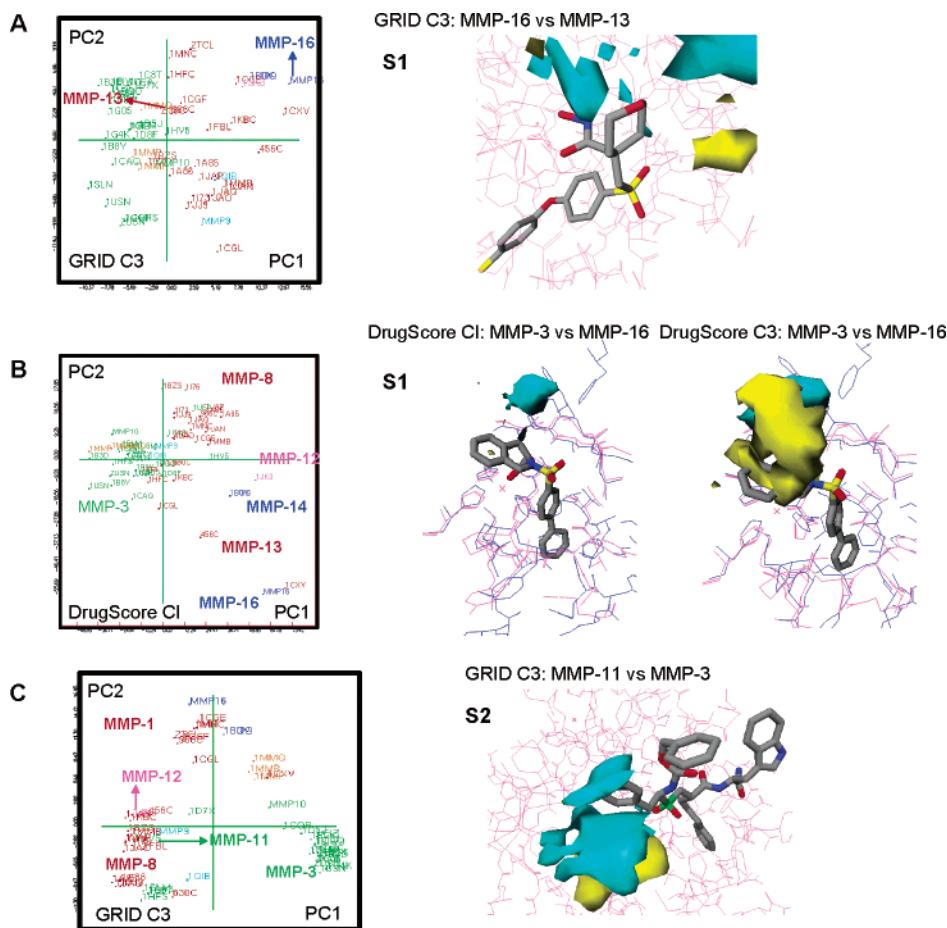
Selectivity differences are displayed in Figure 3F along PC1 for the GRID N1 probe, which shows the strongest contribution to PC1. Differential plots obtained for the other GRID probes have been omitted because these probes produce similar plots (OH, O, C3) or are unable to discriminate between the MMP families (DRY). The crystallographically determined orientation of compound **5** (Chart 1) bound to MMP-3 (PDB code 1BIW) is shown for comparison.[69] Negative contours in PC1 (cyan) indicate a preference for the collagenases and MMP-2, while positive contours in PC1 (yellow) highlight selective interactions

for the remaining metalloproteases. The separation along PC1 is highly determined by residue at position 193 (MMP-3 numbering), which is located on a loop. Both the collagenases and MMP-2 contain a tyrosine at this position, which results in a smaller S3′ pocket compared to the other members containing Thr (stromelysins and MMP-12), Asn (membrane type MMPs), Ile (MMP-7 and TACE), or Gln (MMP-9). For MMP-9 and TACE, the size of the S3′ pocket is also affected by the different lengths and conformations of the loop containing residue 193. Our observations are consistent with the SAR reported for MMP inhibitors binding to the S3′ pocket. Indeed, increasing the size of the P3′ group can lead to as much as a 40-fold increase in binding to MMP-3 and MMP-7 relative to a P3′ methyl group, whereas these modifications cause modest loss of binding to collagenases.[70] It is also noteworthy that interaction of a polar probe (N1, O, OH) close to the ether side chain of compound **5** (Chart 1) is favorable for selectivity versus the collagenases and MMP-2. Also, replacement of the ether of an analogue of compound **5** by an ester results in a dramatic increase in both affinity and selectivity versus MMP-1.[69] Within the solvent exposed S3′ pocket, MMP-3 and -7 display a favorable discrimination with polar probes, which is attributed to the nature of the residue at position 193 (MMP-1, -2, -8, -9, -13, -20/Phe, Tyr; MMP-3, -12/Thr; MMP-7/Ile; MMP14/Asn) and the favorable interaction with the side chain of Asn162 in MMP-3 and -7.

These findings are in good agreement with the DrugScore/ CPCA submodels, as shown in Figure 3G. The most important DrugScore probes for separating the MMP family members with respect to S3′ are chlorine (Cl), sp² and sp³ carbons (C.2, C.3), followed by amide nitrogen (N.am) and then different oxygen probes O.3 and O.2. In Figure 3G, the submodel generated using the most discriminating chlorine probe is displayed with compound **4** (Chart 1) bound to MMP-8 (PDB code 1BZS) as reference. This probe clearly discriminates on the PC1 axis between the collagenase family (red) on the right from the stromelysin family (green), MMP-7 and other MMPs. Only the gelatinase family MMP-2 and -9 (cyan) is split between those two clusters. The main structural reasons for this discrimination agree with the amino acid differences outlined above. The middle panel of Figure 3G indicates regions where favorable interactions with a chlorine probe allow discrimination between MMP-3 (cyan contours) from MMP-8 (yellow contours) along the PC1 axis of the corresponding submodel. The possibility of discriminating within a MMP subfamily is indicated in the right panel highlighting favorable interactions to discriminate MMP-13 (cyan) from MMP-8 (yellow) following the PC2 axis of this submodel.

2.5. Focused GRID/DrugScore CPCA Analysis of MMP Subpockets: S1. Together with the S2 and S3 subsites, the S1 subpocket forms a shallow region bordered on one side by the β strand IV. Substrate binding to the unprimed subsites is generally weak. Only subtle differences are observed between the S1−S3 subsites of the different MMPs. However, a series of thiadiazolyl inhibitors, like compounds **2** and **3** (Chart 1), which bind to the unprimed MMP subsites, exhibit selectivity differences.[31,71] Since the alignment of the left-hand-side binding cavities of TACE with the MMPs is rather poor, we decided to omit TACE for the GRID/CPCA on the unprimed side of the binding site.

The most important GRID probes for separating the different MMPs with respect to the S1 subsite are C3 and O. The first PC in the GRID/PCA and all the individual GRID/CPCA block models slightly separate MMP-16 from the other MMPs, which

Figure 4. (Continued on next page)

form a loose cluster along PC1 (Figure 4A). On the other hand, the second PC cannot discriminate between the different subfamilies of MMPs. The selectivity differences between MMP-16 and MMP-13 are displayed in Figure 4A for the C3 probe, which exhibits the strongest contribution to PC1. The crystallographically determined orientation of compound **6** (Chart 1) bound to MMP-13 (PDB code 830C) is shown for comparison.[60] The separation along PC1 is driven by structural changes at position 163 (MMP-3 numbering). Both MMP-14 and -16 contain a phenylalanine at this position, which is replaced by smaller residues in other MMPs: Asn (MMP-1), Leu (MMP-2, -9, -13), Ile (MMP-8, -11, -12), Val (MMP-3), Thr (MMP-7), Ser (MMP-10). However in the score plot shown in Figure 4A, MMP-14 is separated from MMP-16 as a result of a conformational change of the Phe163 side chain, which makes the MMP-14 S1 pocket larger and hence more similar to the S1 pocket of the other MMPs. However, it remains unclear whether the different conformations of Phe163 in MMP-14 and -16 are significant or result from an artifact of the homology modeling.

The individual DrugScore/CPCA models are in good qualitative agreement with these findings from GRID/CPCA. The most important probes for separating the MMP family members with respect to S1 are chlorine (Cl), followed by sp^2 and sp^3 carbon atom probes (C.2, C.3).

In Figure 4B, the Cl probe derived submodel is displayed, which clearly discriminates MMP-16 and, to a lower extent, MMP14 (PDB codes 1BQQ and 1BUV), MMP-11 (PDB code 1HV5) plus one single mouse MMP-13 conformation (PDB code 1CXV[72]). This discrimination is mainly related to the

characteristic residue Phe163 present in membrane-type MMPs, while MMP-11 has an Ile residue at this position. Although the mouse MMP-13 structure also has a Leu at this position, it shows a conformational rearrangement of the neighboring residue Tyr155 (MMP-3 numbering), which now is oriented toward the S1 pocket. This contrasts with two other MMP-13 structures from the human orthologue (PDB codes 456C and 830C). This conformational difference is also related to a slightly different orientation of the tetrahydropyrane scaffold of compound **6** (Chart 1) bound to the mouse MMP-13 structure (PDB code 1CXV). However, because these three MMP-13 structures are obtained in complex with rather similar ligands, this conformational difference could also result from species differences between mouse and human, as both sequences share only 93% identify, while no mutation is obvious in the neighborhood of this subpocket.

2.6. Focused GRID/DrugScore CPCA Analysis of MMP Subpockets: S2. The shape of the S2 subpocket is strongly influenced by the N-terminal amino acids in individual members of the MMP family. In some inspected X-ray structures, this site is extremely solvent-exposed. The most important GRID probes for separating the different MMPs with respect to the S2 subsite are C3 followed by DRY, N1, and OH probes, while the O probe is less important for discrimination. The first PC in the PCA and all the individual CPCA block models (Figure 4C) but the O one separate all the collagenases but the mouse MMP-13 (PDB code 1CXV), the gelatinases, MMP-11, MMP-12, and MMP-16 (negative PC1 scores) from all of the MMP-3 but five structures (PDB codes 1SLM, 1C8T, 1UEA, 1HFS, and 1D7X), the MMP-7, the MMP-10, the mouse MMP-13
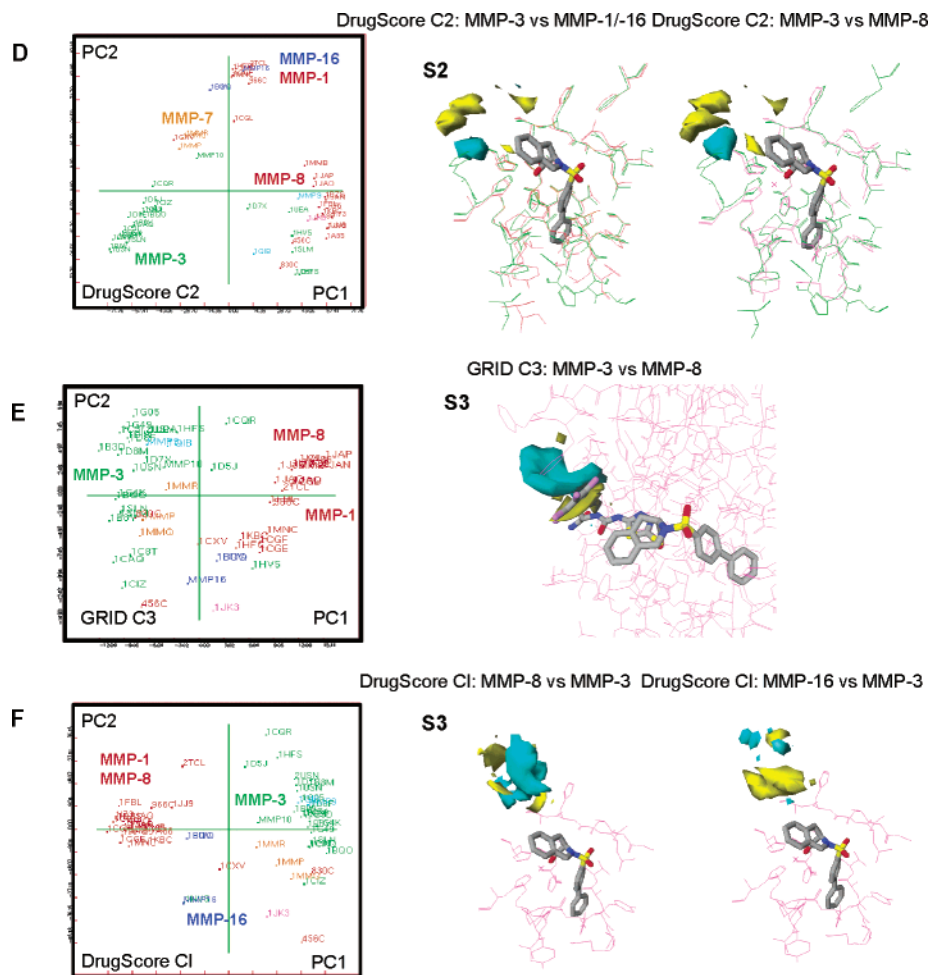
Figure 4. CPCA submodels for MMP nonprime pockets (S1 (A, B), S2 (C, D), S3 (E, F)) obtained from GRID and DrugScore. Middle and right panels highlight regions of the nonprime pockets where selectivity between different MMPs can be gained using a given probe. Compounds **6**, **4**, **7**, and **2** (Chart 1) bound to MMP-13 (PDB code 830C), MMP-8 (PDB code 1BZS), MMP-11 (PDB code 1HV5), and MMP-3 (PDB code 1USN) are shown as reference (A, B, D−F, C, E, respectively). (A) CPCA score plot for the GRID C3 probe (left panel); favorable interactions to discriminate the S1 pockets of MMP-13 (PDB code 830C, cyan) and MMP-16 (homology model, yellow) using the GRID C3 probe (right panel). (B) CPCA score plot for the DrugScore Cl probe (left panel), favorable interactions to discriminate the S1 pocket of MMP-3 (PDB code 1USN, cyan) and MMP-16 (homology model, yellow) using the DrugScore Cl probe (middle panel); favorable interactions to discriminate the S1 pocket of MMP-3 (PDB code 1USN, cyan) and MMP-16 (homology model, yellow) using the DrugScore C.3 probe (right panel). (C) CPCA score plot for the GRID C3 probe (left panel); favorable interactions to discriminate the S2 pocket of MMP-11 (PDB code 1HV5, cyan) and MMP-3 (PDB code 1USN, yellow) using the GRID C3 probe (right panel). (D) CPCA score plot for the DrugScore C.2 probe (left panel), favorable interactions to discriminate the S2 pocket of MMP-3 (PDB code 1USN, cyan) and MMP-1/16 (PDB code 1CGE and homology model, yellow) using the DrugScore C.2 probe (middle panel), favorable interactions to discriminate the S2 pocket of MMP-3 (PDB code 1USN, cyan) and MMP-8 (PDB code 1BZS, yellow) using the DrugScore C.2 probe (right panel). (E) CPCA score plot for the GRID C3 probe (left panel), favorable interaction to discriminate the S3 pocket of MMP-3 (PDB code 1USN, cyan) and MMP-8 (PDB code 1BZS, yellow) using the GRID C3 probe (right panel). (F) CPCA score plot for the DrugScore Cl probe (left panel); favorable interactions to discriminate between MMP-8 (PDB code 1BZS, cyan) and MMP-3 (PDB code 1USN, yellow) using the DrugScore Cl probe, favorable interactions to discriminate between MMP-16 (homology model, cyan) and MMP-3 (PDB code 1USN, yellow) using the DrugScore Cl probe.

(PDB code 1CXV), and the MMP-14 structures (positive PC1 scores). The second PC discriminates between a group of structures showing negative PC2 scores (MMP-2 (PDB code 1QIB), four MMP-3 (PDB codes 1SLM, 1C8T, 1UEA, and 1HFS), all the MMP-8 but one (PDB code 1MNC), MMP-11, MMP-12, the human MMP-13 (PDB codes 456C and 830C)) and another group with positive PC2, formed by the MMP-1, MMP-7, the mouse MMP-13 (PDB code 1CXV), one MMP-8 (PDB code 1MNC), and the membrane type MMP (MMP-14 and MMP-16).

The MMP subfamily selectivity differences are plotted in Figure 4C for PC1 for the C3 probe, which both strongly contribute to PC1 and PC2. The experimental orientation of compound **7** (Chart 1) bound to MMP-11 (PDB code 1HV5) is displayed for comparison. Negative contours in PC1 (cyan)

indicate a preference for MMP-11 and the neighboring proteins, while positive contours in PC1 (yellow) highlight selective interactions for MMP-3 and the neighboring proteins.

Three main structural changes determine the separation of the MMP structures in the PC1−PC2 score plot. First of all, the residue in position 210 (MMP-3 numbering) is poorly conserved among the MMP family: Ser (MMP-1), Glu (MMP-2, MMP-14, and MMP-16), Phe (MMP-3 and MMP-10), Gly (MMP-7 and MMP-12), Ala (MMP-8), Asp (MMP-9 and MMP-13), and Gln(MMP-11). Different conformations adopted by the Phe210 side chain are responsible for the split observed in the PC1−PC2 score plots among the MMP-3 structures. Another variable amino acid is located in position 169 (MMP-3 numbering): Gln(MMP-1 and MMP-8), Ala (MMP-2, MMP-3, and MMP-7), Pro (MMP-9, MMP-10, and MMP-13), Phe

(MMP-11, MMP-14, and MMP-16), or Gly (MMP-12). Finally, structural variations around positions 86 and 87, part of the N terminal of the MMPs, also account for the separation of the MMP structures shown in Figure 4C. However, the coordinates of residues 86 and 87 are missing or this segment is poorly aligned for several proteins of the data set. This artificially increases the differences in the score plot. It is also noteworthy that for the MMP-3 structures separated from the main MMP-3 cluster, residues 86 and 87 are either missing or poorly aligned.

Again, the individual DrugScore/CPCA models are in good agreement with these GRID/CPCA analyses. The most important probes for separating the MMP family members with respect to S2 are of hydrophobic nature, like sp^2 and sp^3 carbon atom probes (C.2, C.3) followed by chlorine (Cl). In contrast, the amide nitrogen (N.am) probe and different oxygen probes O.3 and O.2 are less important for discriminating between MMPs in this subsite.

The discrimination of MMP-3 and other clusters is due to the above-mentioned amino acid differences present in this solvent exposed subpocket. The middle panel of Figure 4D indicates regions where favorable interactions with a C.2 probe allow discriminating between MMP-3 (yellow contours) and the cluster of MMP-1 and -16 structures (cyan). This figure also displays the corresponding binding sites for MMP-3 (PDB code 1BIW) in green and for MMP-1 (PDB code 2TCL) in red, while compound **4** (Chart 1) as bound to MMP-8 (PDB code 1BZS) is shown for reference. The possibility of discriminating MMP-3 from MMP-8 and other MMPs in this broad cluster with positive PC1 values is indicated in the right panel of Figure 4D. Here, favorable interactions to MMP-3 are again displayed in yellow, while cyan contours indicate favorable interactions to MMP-8 and other members of this cluster. Again, the protein structures for MMP-3 (PDB code 1BIW in green) and MMP-8 (PDB code 1BZS in red) are shown for comparison. The main cyan colored contour is located at a position in S2, occupied by the Phe210 side chain in most MMP-3 structures. As discussed above, this residue is poorly conserved in the different MMPs.

2.7. Focused GRID/DrugScore CPCA Analysis of MMP Subpockets: S3. The S3 pocket is a hydrophobic cleft, with proline as the preferred binding group in MMP substrates.[73] The crystal structure of the left-hand side peptidic inhibitor Pro-Leu-Gly-NHOH bound to MMP-8 illustrates the tight fit between the proline side chain and the S3 subsite.[49] The shape of the S3 pocket is defined by amino acids 155, 166, and 168 (MMP-3 numbering).

The five GRID probes exhibit similar contributions to the GRID/CPCA model, obtained for the S3 pocket. The first PC in the PCA and all the individual CPCA block models (Figure 4E) separates MMP-1, MMP-8, MMP-11, and the membrane type MMPs in different clusters with positive PC1 scores from MMP-2, MMP-3, MMP-7, MMP-9, MMP-10, MMP-12, and MMP-13, which are spread along PC2 with negative PC1 scores. This discrimination along PC1 is mainly driven by sequence differences at position 155 (MMP-3 numbering), which is occupied by an aromatic amino acid in the structures with negative PC1 scores (Tyr in all the structures but MMP-12, His in MMP-12), by a nonaromatic amino acid in the structures with positive PC1 scores (Ser for MMP-1, -8, -16, Leu for MMP-11, Thr for MMP-14). As a result, the S3 pocket of MMP-3 and its neighbors in the PCA score plots is smaller and more hydrophobic than the corresponding pocket in MMP-1 and the other structures with positive PC1 scores (Figure 4E). Position 168 contains either a Phe (MMP-1, -2, -8, -9, -11, -12, -13) or a Tyr (MMP-3, -7, -10, -14, -16), which affects the

hydrogen-bonding properties of the S3 pocket (Figure 4E). The separation along PC1 is consistent with the selectivity profile of the thiadiazole MMP inhibitors such as compound **2** (Chart 1), which exhibits nanomolar activity on MMP-3 (IC$_{50}$ = 18 nM) while inactive on MMP-1.[31,71] Indeed, its phenyl ring, which matches the negative CPCA differential contours for the DRY probe (selective interaction with MMP-3), is involved in favorable stacking interactions with the aromatic ring of Tyr155 in MMP-3. On the other hand, structural changes in the S3 pocket cannot explain its 166-fold weaker activity for MMP-2. Instead, the main structural difference between MMP-3 and MMP-2 occurs in the S2 pocket at position 169, which contains a Phe in MMP-3 and a Glu in MMP-2. Assuming the same binding mode of compound **2** to MMP-2 as the one observed for MMP-3, none of its H-bonding group could form an H bond with the side chain of Glu210, which might explain the weaker binding affinity for MMP-2.

Again, the individual DrugScore/CPCA models are found to be in good agreement with the GRID/CPCA results. Hydrophobic probes are again more important for separating MMP family members with respect to the S3 subpocket. The amide nitrogen (N.am) probe and different oxygen probes O.3 and O.2 are less important for discrimination.

In Figure 4F, the Cl probe derived DrugScore/CPCA submodel is displayed. It separates the cluster of MMP-1 and -8 structures with negative PC1 scores from all other MMPs. The other MMPs are separated into one large group containing all MMP-3 structures plus MMP-2, -9, and -10. In addition, separate clusters are observed for MMP-7, MMP-12, MMP-14, MMP-13, MMP-16, while the MMP-13 structures are spread over a larger region in this PC1−PC2 score plot in the lower right area.

This discrimination of MMP-1 and -8 as members of the collagenase family is mainly due to the above-mentioned residue differences at positions 155 and 168 (MMP-3 numbering) in this S3 subpocket. The middle panel of Figure 4F highlights regions where favorable interactions with a chlorine probe discriminate the collagenases MMP-1 and -8 (cyan contours) from the remaining clusters of MMPs including MMP-3 (yellow). This comparison again is shown using compound **4** (Chart 1) bound to MMP-8 (PDB code 1BZS) as a reference for visualization. This picture is qualitatively similar to score plots derived using other probes such as sp^2 and sp^3 carbon, while the clustering in these plots differ in comparison to the results from polar DrugScore probes. MMP-3 contains two hydrophobic residues Tyr155 and 168 in this area interacting with the yellow contour region in Figure 4F (middle panel), while Ser and Phe replace those amino acids in MMP-8. Similar mutations in the S3 pocket of other MMPs form the basis for the discrimination by hydrophobic probes.

The possibility of discriminating MMP-16 from MMP-3 and other MMPs along PC2 is indicated in the right panel of Figure 4F. Here, favorable interactions with MMP-3 are again displayed in yellow, while cyan contours indicate favorable interactions with MMP-13 and MMP-12. Both yellow and cyan contour regions are located close to the Tyr155 (MMP-3 numbering) residue.

2.8. Analysis of MMP Inhibitor Selectivity. In the following chapter, the GRID and DrugScore/CPCA models for MMP binding sites serve to rationalize experimental binding affinity differences for selected inhibitors. The discovery and optimization of MMP inhibitors are increasingly driven by the need for lead structures having a defined pharmacological and selectivity profile. Recent reviews have summarized structural and inhibi-
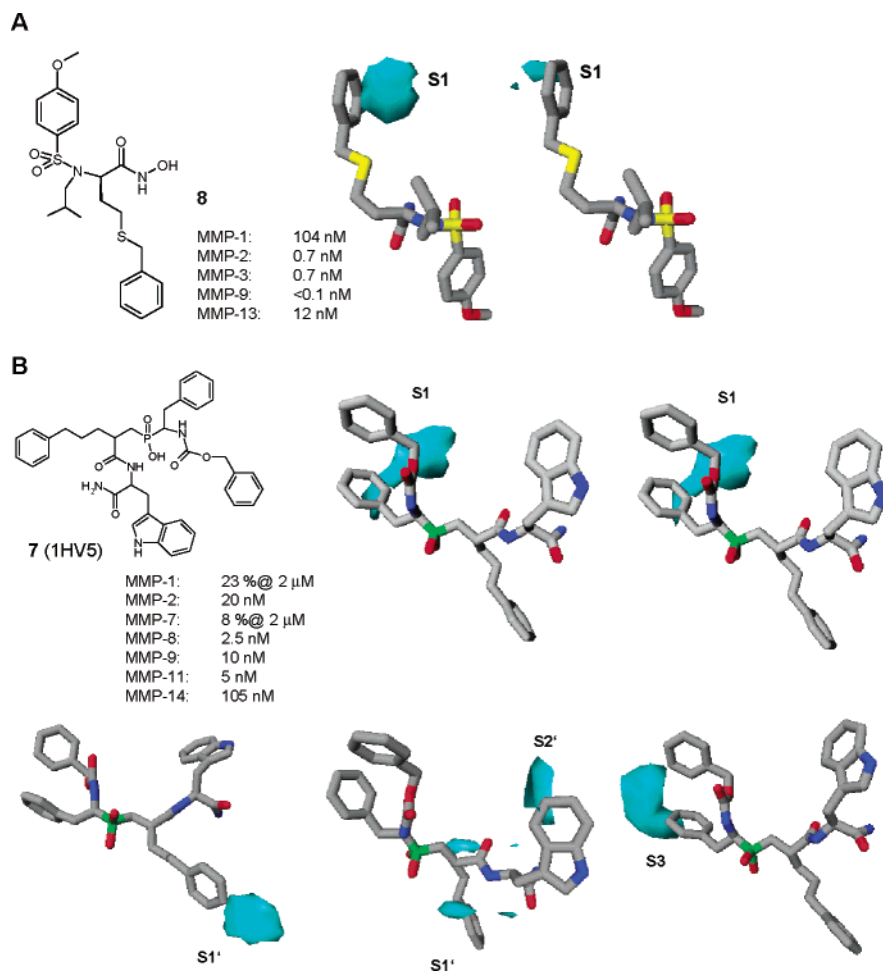
Figure 5. (Continued on next page)

tion properties of some novel MMP inhibitors with selectivity to many related MMPs.[74,41] Furthermore, disappointing results from clinical trials in cancer have raised questions regarding the importance of selectivity for minimizing undesirable side effects.[75] Several MMP inhibitors with a distinct selectivity profile have emerged, although it appears to be challenging to selectively interact only with one member of this target family while sparing all related members. However, the optimal MMP inhibitor profile for diseases with MMP involvement has remained elusive so far.[41] Consequently the following discussion on applications of the protein-derived models provides information for unraveling essential selectivity differences from the perspective of the ligands. To this end, selected examples from the medicinal chemistry literature were analyzed in detail.

For all inhibitors in this section a hypothesis about the likely binding mode within the MMP binding site has been developed either using X-ray crystallographic information in the PDB or using automated docking into MMP-2 (PDB code 1QIB), MMP-3 (PDB code 1CAQ), or MMP-8 (PDB code 1BZS) X-ray structures. The fundamental assumption is that the binding mode does not significantly change in different MMP binding sites. This assumption is supported by X-ray structures of batimastat bound to MMP-8, MMP-12, and MMP-16 (PDB codes 1MMB, 1JK3, 1RM8, respectively). It should be noted that a quantitative comparison of IC$_{50}$ values from different laboratories with differing assay conditions is not feasible, while the qualitative analysis of SAR and selectivity trends between different MMPs studied in the same laboratory is a reasonable approach for extracting structural discriminants for selectivity. As for the
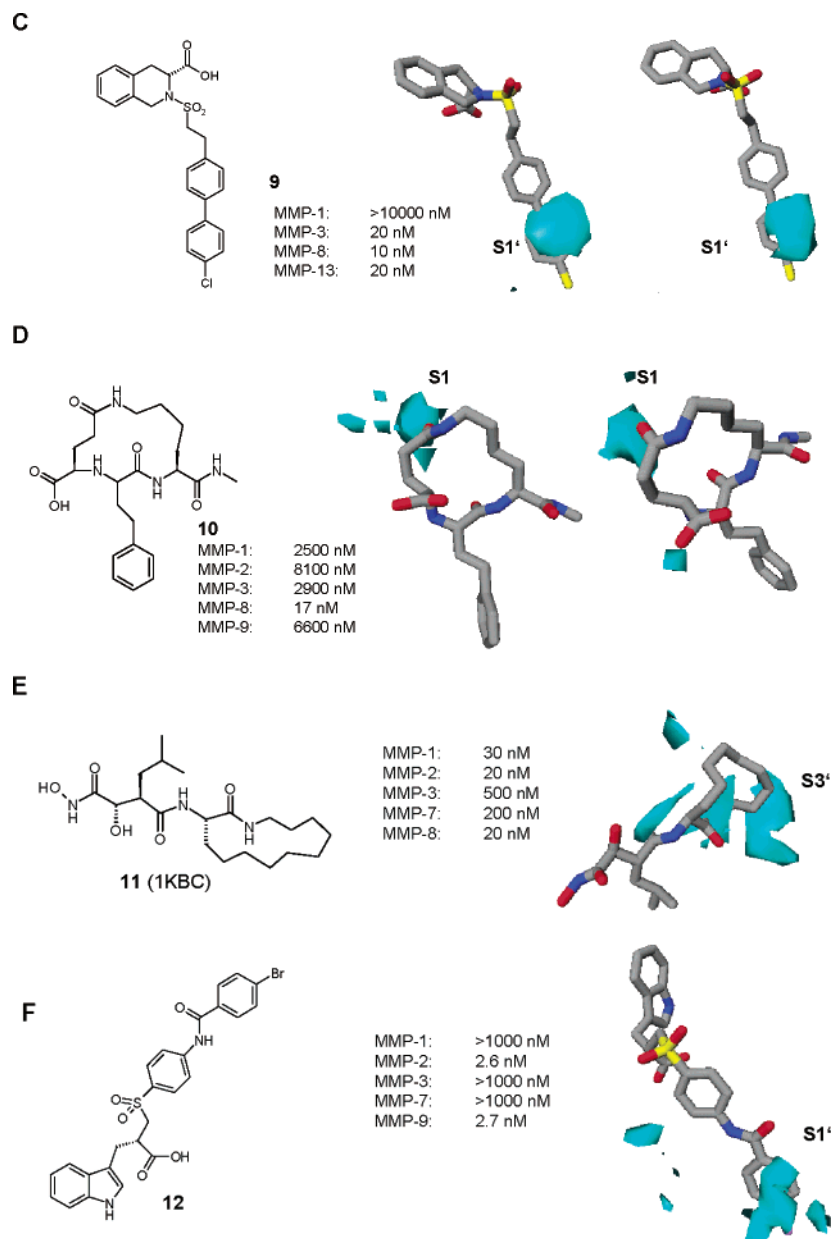
comparison of protein subsites, this ligand-focused analysis is carried out using the GOLPE active plot option to focus on relative differences. For simplification, only the ligand structure is shown for orientation without protein residues, while all contours were obtained from analyzing protein binding sites.

2.8.1. *N*-Arylsulfonyl Homocysteine Hydroxamatic Acids. Hanessian et al. disclosed a series of inhibitors based on an *N*-arylsulfonyl homocysteine hydroxamic acid scaffold.[76,77] This framework allows for orientation of appropriate substituents toward the MMP S1, S1′, and S2 subpockets. Rigidization yielded substituted D-proline hydroxamic acids with distinct selectivity profiles.[78] These data allow correlation of observed selectivity profiles with substituents in distinct subpockets.

This is illustrated for the hydrophobic S1 pocket surrounded by Tyr155, His166, and Tyr168 (MMP-3 numbering). The lead compound **8**[78] is shown in Figure 5A with its likely binding mode from flexible docking into MMP-3. The following activities are reported (IC$_{50}$): MMP-1, 104 nM; MMP-2, 0.7 nM; MMP-3, 0.7 nM; MMP-9, <0.1 nM; MMP-13, 12 nM. This compound exhibits a distinct selectivity profile favoring MMP-9 over MMP-2 and -3, while this molecule displays a significantly lower affinity for MMP-1 and -13.

Although the previous discussion suggested that the S1 pocket is not much involved in achieving selective inhibition, biological data for this series point to some discriminating interactions in this area. In the left panel of Figure 5A, compound **8** is displayed with cyan contours from the DrugScore/CPCA model for the S1 pocket and the sp^2 carbon probe (C.2). The contour region close to the *S*-benzyl ring indicates that hydrophobic groups

C

9

MMP-1:	>10000 nM
MMP-3:	20 nM
MMP-8:	10 nM
MMP-13:	20 nM

D

10

MMP-1:	2500 nM
MMP-2:	8100 nM
MMP-3:	2900 nM
MMP-8:	17 nM
MMP-9:	6600 nM

E

MMP-1:	30 nM
MMP-2:	20 nM
MMP-3:	500 nM
MMP-7:	200 nM
MMP-8:	20 nM

11 (1KBC)

F

| MMP-1: | >1000 nM |
MMP-2:	2.6 nM
MMP-3:	>1000 nM
MMP-7:	>1000 nM
MMP-9:	2.7 nM

12

Figure 5. (Continued on next page)

with this or related atom types favorably discriminate MMP-9 from MMP-13, which corresponds to the experimentally observed 120-fold difference in affinity. The middle panel highlights a similar region located at the distal ring for some selective inhibition of MMP-9 versus MMP-3, as extracted from the DrugScore/CPCA analysis for an sp^2 carbon. This result is consistent with the binding affinity differences between MMP-3 and MMP-9 reported for compound **8** (Figure 5A). In particular, the substitution of the *S*-benzyl group with a para phenyl group increases the selectivity ratio MMP-9/MMP-3 to 100-fold. This is also related to the limited size of the S1 pocket in MMP-3. Docking indicates that this site is perfectly filled by the *S*-benzyl group. In contrast, substitution of all protons in the benzyl ring with the halogen F or replacement of the phenyl ring by less hydrophobic rings is detrimental for selectivity. This corresponds to the observed potential for discrimination from analyzing DrugScore sp^2 and sp^3 carbon and related GRID/CPCA models, while the DrugScore Cl probe does not result in any discrimination.

2.8.2. Phosphinic Pseudotripeptides. Vassiliou et al. described a series of phosphinic pseudotripeptides as MMP inhibitors with distinct selectivity profiles.[79] The peptidic scaffold allows the directing of different substituents toward different subpockets in order to explore their potential to selectively interact with only a few from a panel of seven MMPs. The lead structure **7** (Chart 1) with selectivity for MMP-11 and -8 over the remaining members was crystallized in MMP-11 (PDB code 1HV5), providing insights into the binding mode of MMP transition state mimics.[80] The following activities are reported (K_i values or percent inhibition): MMP-1, 23% at 2 μM; MMP-2, 20 nM; MMP-7, 8% at 2 μM; MMP-8, 2.5 nM; MMP-9, 10 nM; MMP-11, 5 nM; MMP-14, 105 nM.

The upper middle panel of Figure 5B shows the experimental binding mode of **7** in MMP-11 with cyan contours highlighting selectivity regions for MMP-11 versus MMP-1, -14, and others in the S1 pocket from the DrugScore/CPCA C.2 model. The upper right panel of Figure 5B indicates similar cyan selectivity regions for MMP-11 versus MMP-7 from the same model.
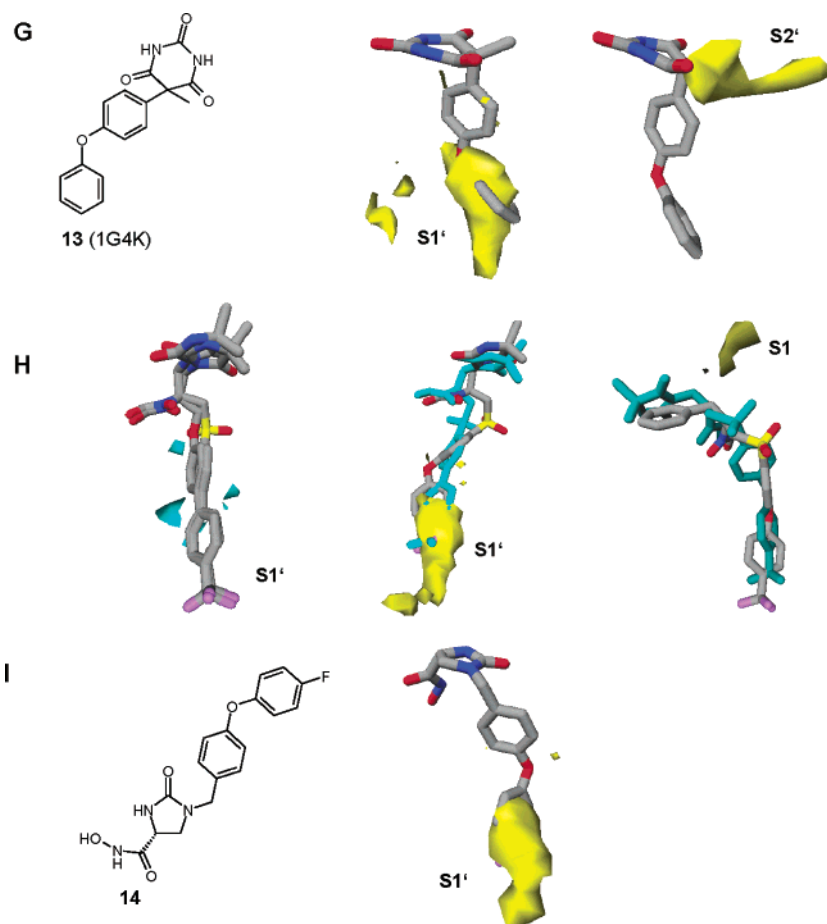
Figure 5. Binding mode from X-ray crystallography or from flexible docking for representative examples from the medicinal chemistry literature. The PC1 or PC2 differential plots obtained for selected GRID or DrugScore probes are also displayed to highlight regions of the MMP binding site where selectivity for a given MMP can be gained. For each example, the 2D structure of the cocrystallized or docked structure is shown in the far left panel; its proposed binding mode with the corresponding differential contour is displayed in the other panels. These plots are discussed in details in section 3.8. The protein structure has been omitted for clarity. (A) Compound **8** docked in MMP-3 (PDB code 1CAQ) with DrugScore/ CPCA differential contours obtained for the C.2 probe. These contours highlight differences between the S1 pockets of MMP-9 and -13 (homology model, PDB code 830C; left panel) and the S1 pockets of MMP-9 and -3 (homology model and PDB code 1CAQ; right panel) (B) Compound **7** bound to MMP-11 (PDB code 1HV5, upper panels, lower left and right panels) and docked in MMP-8 (PDB code 1BZS, lower middle panel). All the DrugScore/CPCA differential contours were obtained for the C.2 probe. These contours highlight differences between the S1 pockets of MMP-1 and -11 (PDB codes 1CGL and 1HV5; upper middle panel), the S1 pockets of MMP-7 and -11 (PDB codes 1MMP and 1HV5; upper right panel), the S1′ pocket of MMP-1 and -11 (PDB codes 1CGL and 1HV5; lower left panel), the S1′ and S2′ pockets of MMP-8 and -14 (PDB codes 1BZS and 1BQQ; lower middle panel), and the S3 pockets of MMP-7 and -11 (PDB codes: 1MMP and 1HV5; lower right panel). (C) Compound **9** docked in MMP-8 (PDB code 1BZS) with DrugScore/CPCA contours obtained for the C.2 (middle panel) and Cl (right panel) probes. These contours highlight differences between the S1′ pockets of MMP-1 and -8 (PDB codes 1CGE and 1BZS). (D) Compound **10** docked in MMP-8 (PDB code 1BZS) with DrugScore/CPCA differential contours obtained for the Cl (middle panel) and O.2 (right panel) probes. These contours highlight differences between the S1 pocket of MMP-3 and -8 (PDB codes 1CAQ and 1BZS). (E) Compound **11** bound to MMP-8 (PDB code 1KBC) with DrugScore/CPCA differential contours obtained for the C.3 probe. These contours highlight differences between the S3′ pocket of MMP-3 and -8 (PDB codes 1CAQ and 1KBC). (F) Compound **12** docked in MMP-2 (PDB code 1QIB) with DrugScore/CPCA differential contours plot for the O.2 probe. These contours highlight differences between the S1′ pockets of MMP-2 and -3 (PDB codes 1QIB and 1CAQ). (G) Compound **13** bound to MMP-3 (PDB code 1G4K) with DrugScore/CPCA differential contours obtained for the C.3 probe. These contours highlight differences between the S1′ (middle panel) and S2′ (right panel) of MMP-2 and -3 (PDB codes 1QIB and 1G4K). (H) Retrohydroxamates from Table 3 docked in MMP-2 (PDB code 1QIB) with GRID/CPCA differential plots obtained for the N1 (left panel) and C3 (middle and right panels). These contours highlight differences between the S1′ and S1 pockets of MMP-1 and -2 (PDB codes 1CGE and 1QIB). (I) Compound **14** docked in MMP-3 (PDB code 1CAQ) with GRID/CPCA differential contour plot obtained for the C3 probe. These contours highlight differences between the S1′ pockets of MMP-3 and -13 (PDB codes 1CAQ and 830C).

Those cyan contours in both panels indicating MMP-11 selectivity are located next to the carbamate linker of **7** close to Ile180 in MMP-11 and the phenylalanine side chain close to Leu172. These contours are located in the S1 and S2 pockets, respectively. This is in good agreement with the reported MMP-11 preference to accommodate hydrophobic groups in its S1, S1′, and S2′ positions.[80,81] In contrast, the benzyl part of the benzyloxycarbonyl group is exposed to the solvent and not clearly defined in the electron density map. Consequently this part is not close to any selectivity region. However, a rigidization

by introducing hydrophobic indole-2-carboxamide derivatives significantly increases affinity and selectivity toward MMP-11.[80]

In the lower left panel of Figure 5B, selectivity regions for MMP-11 in the S1′ specificity pocket are shown on the basis of the DrugScore/CPCA C.2 model. A preference for aromatic carbons to discriminate MMP-11 from MMP-1, -7, and others is indicated by contours close to the edge of the propylphenyl ring. The S1′ subsite in MMP-11 is more like a channel, which partially accommodates this phenylpropyl group. The analysis

of the MMP-11/**7** X-ray structure[81] and SAR trends[80,82] also suggests a preferred position for the phenyl ring in the S1′ pocket.

The lower middle panel of Figure 5B provides information about the S2′ pocket with cyan selectivity regions at the tryptophan indole C5 position from the DrugScore/CPCA C.2 model. This model allows discriminating MMP-8 (2.5 nM) from MMP-14 (105 nM) and others. Interestingly, MMP-2 and -9 are located between both extrema in the DrugScore/CPCA plot. This observation agrees with their medium binding affinity of 20 and 10 nM, respectively. This contour region alone is related to the Gly180 Cα and Ile179 side chains in MMP-8 and -11 and explains a significant part of the binding affinity toward these MMPs. Replacing tryptophan in compound **7** by alanine reduces the selectivity MMP-8/-14 from 42-fold to 12-fold, while MMP-11 activity is dramatically decreased to 20% at $1\mu M$.[80,81]

Finally the lower right panel in Figure 5B highlights, in cyan, selectivity regions in the S3 pocket from the DrugScore/CPCA C.2 model. This region located at the phenylalanine ring discriminates MMP-11 from MMP-7 and others on the basis of hydrophobic interactions. The corresponding side chain is involved in a favorable hydrophobic protein−ligand contact with Leu172 in MMP-11, which obviously contributes to selectivity. Hence, the observed selectivity profile of this lead compound **7** and several derivatives is determined by a combination of several primary hydrophobic factors in different MMP subsites. These results suggest that there is no simple solution to selectivity, but there is the possibility of capturing several positive effects.

2.8.3. 1,2,3,4-Tetrahydroisoquinoline-3-carboxylates. The design and structure−activity relationship of a series of 2-arylsulfonyl-1,2,3,4-tetrahydroisoquinoline-3-carboxylates and hydroxamates as MMP-8 inhibitors were previously described.[82] The compounds described in ref 82 were designed using multiple 3D QSAR models.[21,22] Incorporating novel S1′-directed substituents resulted in a series of carboxylate-based MMP-8 inhibitors with selectivity against MMP-1. The structural reason for selectivity is related to the discriminating properties of the S1′ specificity pocket, as discussed above. This is illustrated using the binding mode of compound **9** docked into MMP-8, as shown in Figure 5C with contours indicating selectivity regions within S1′. Cyan contours indicate favorable regions for selectivity in S1′ for MMP-8, -3, and -13 versus MMP-1 for C.2 (middle panel) and a Cl atom type (right panel) from the DrugScore/CPCA analysis. These contours regions are in good agreement with the experimental binding affinity profile, which is reported for compound **9** (IC$_{50}$): MMP-1, >10000 nM; MMP-3, 20 nM; MMP-8, 10 nM; MMP-13, 20 nM. The distal chlorophenyl ring is directly located within the cyan selectivity region responsible for this discrimination, which also corresponds to SAR trends in the literature.[21,22,82] The MMP-3/-8 IC$_{50}$ values for compound **9** agree with the conclusions of a previously published 3D QSAR model for MMP-3/-8 selectivity.[21,22]

2.8.4. Macrocyclic Lactams between S1 and S2′. Cherney et al. described a series of macrocyclic lactams[83] as selective inhibitors of MMP-8 by cyclization of substituents directed toward the MMP S1 and S2′ subpockets from a precursor molecule.[84] The most selective 14-membered lactam (compound **10**, Figure 5D) was reported to have the following binding affinities (K_i): MMP-1, 2500 nM; MMP-2, 8100 nM; MMP-3, 2900 nM; MMP-8, 17 nM; MMP-9, 6600 nM. The most likely binding mode of this inhibitor **10** from docking in MMP-8 is
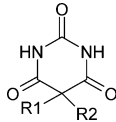
shown in Figure 5D in combination with selectivity regions obtained from the DrugScore/CPCA analysis. The cyan contours in the middle panel indicate selectivity regions from the analysis based on the DrugScore chlorine probe. The favorable contour region discriminating MMP-8 from MMP-3 and MMP-1 on the basis of hydrophobic interactions in the S1 area is located at the macrocyclic lactam bridge. This latter is close to the MMP-8 residues Phe153, Ile159, and His162. The right panel of Figure 5D highlights selectivity regions from the DrugScore/CPCA O.2 probe. These regions also indicate possibilities for discrimination between MMP-8 (cyan) versus MMP-3 and others. The contour regions collectively agree with the previous hypothesis about the influence of the S1−S2′ linkage to determine MMP-8 selectivity because precursor molecules without this linkage do not exhibit any significant selectivity.[84]

2.8.5. Macrocyclic Lactam BB-1909 between S2′ and S3′. Betz et al. reported the X-ray structure of the complex between MMP-8 and compound **11** (PDB code 1KBC, Figure 5E).[85] This inhibitor **11** with a macrocyclic lactam bridging the S2′ and S3′ subsites is located in a different region compared to compound **10**. It binds to the S1′, S2′, and S3′ subsites of different MMPs with the following binding affinities (IC$_{50}$): MMP-1, 30 nM; MMP-2, 20 nM; MMP-3, 500 nM; MMP-7, 200 nM; MMP-8, 20 nM. Hence, there is only a moderate 10- to 25-fold selectivity difference between the MMPs tested.
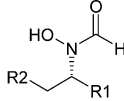
In Figure 5E the crystallographic binding mode of compound **11** (PDB code 1KBC) is shown in combination with cyan contours indicating a selectivity region in S3′ based on the DrugScore/CPCA model using the C.3 probe. Cyan contours in this S3′ pocket close to the macrocyclic lactam bridge indicate a favorable region for aliphatic carbons to discriminate between one cluster consisting of MMP-8, -2, and -3 (cyan) versus MMP-3 and -7 in another cluster. However, this and other probes do not indicate any complete separation between one MMP from all other members of this family, in agreement with the experimental selectivity profile. Hence, the moderate 10- to 25-fold selectivity difference between both clusters of the MMP family is mainly due to discriminating hydrophobic interactions in the S3′ pocket. This is also in good agreement with the observation of asparagine residues in MMP-3 and -7 situated in the S2′ and S3′ pockets, which results in weaker protein−ligand interactions with the methylene bridge in both cases.
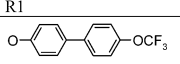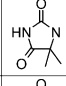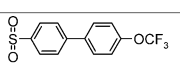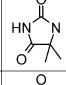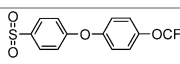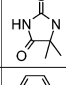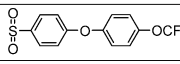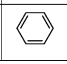
2.8.6. *N*-Sulfonylamino Acids. Tamura et al. described a series of selective MMP-2 and -9 inhibitors based on an *N*-sulfonylamino acid scaffold.[86] For the lead compound **12** (Figure 5F), the following biological data have been reported (IC$_{50}$): MMP-1, >1000 nM; MMP-2, 2.6 nM; MMP-3, >1000 nM; MMP-7, >1000 nM; MMP-9, 2.7 nM. The most likely docking mode of compound **12** in MMP-2 is shown in Figure 5F in combination with contour regions in the S1′ pocket next to the amide group linking both S1′ directed phenyl rings. These regions were obtained from analyzing the DrugScore/CPCA model for the S1′ pocket and the O.2 probe. They indicate favorable interactions for discrimination of gelatinases, MMP-2 in particular, versus MMP-3, -1, -7, and other members of this target family. Interestingly this contour region is close to the amide carbonyl group of compound **12**. Because an X-ray structure of a related side chain in a gelatinase is lacking, the binding mode is deduced from flexible docking and might contain inaccuracies, which might explain the slight deviation between inhibitor atoms and the protein derived contour. However, also in this case, the CPCA derived contours are

Table 2. MMP Inhibition Data (IC$_{50}$, μM) for Selected 5,5-Disubstitutedpyrimidine-2,4,6-triones[a]

R1	R2	MMP-3	MMP-2	MMP-9
Me(CH$_2$)$_5$	Ph	30	1.3	0.33
Me	PhOPh	2	0.081	0.052
Me(CH$_2$)$_5$	PhOPh	2	0.021	0.018
CH$_2$OCH$_2$Ph	PhOPh	0.93	0.019	0.017

[a] Data are from ref 87.

Table 3. MMP Inhibition Data (IC$_{50}$, nM) for Selected Phenoxyphenyl Sulfone Retrohydroxamates[a]

R1	R2	MMP-1	MMP-2
O—⟨ ⟩—⟨ ⟩—OCF$_3$	(barbituric, dimethyl)	4600	3.7
O=S=O—⟨ ⟩—⟨ ⟩—OCF$_3$	(barbituric, dimethyl)	82	0.86
O=S=O—⟨ ⟩—O—⟨ ⟩—OCF$_3$	(barbituric, dimethyl)	820	1.3
O=S=O—⟨ ⟩—O—⟨ ⟩—OCF$_3$	(phenyl)	> 50000	7.4

[a] Data are from ref 89.

useful in the analysis and understanding of structural reasons for selective interactions with only a few members of the MMP family.

2.8.7. 5,5-Disubstituted Pyrimidine-2,4,6-triones. A group at Roche described 5,5-disubstituted pyrimidine-2,4,6-triones showing selectivity for MMP-2 and -9 over MMP-3.[87] As shown in Table 2, the selectivity for MMP-2 and -9 over MMP-3 depends on the size of the R1 and R2 substituents, inhibitors with larger substituents being more selective over MMP-3. The crystal structure of one representative of this class in complex with MMP-3 (PDB code 1G4K) reveals that substituents R1 and R2 are directed toward the S2′ and S1′ subpockets, respectively.[88] The R1 and R2 substituents of compound **13** bound to MMP-3 overlap with positive contours of the PC2 and PC1 differential plots obtained for the GRID C3 probe (Figure 5G, middle and right panels). These positive contours highlight regions of the S1′ and S2′ subpockets where increasing steric bulk contributes to enhance selectivity for MMP-2 and -9 over MMP-3.

2.8.8. Retrohydroxamates. A group at Abbott exploited two subpockets, S1′ and S1, to achieve selectivity for MMP-2 over MMP-1.[89] Their starting point, which had a retrohydroxamate as Zn binder and a biaryl ether binding to the S1′ subpocket, was selective for MMP-2 over MMP-1 (Table 3). To further probe the structure−activity relationships for this class, they replaced the ether by a sulfone, which resulted in a loss of selectivity for MMP-2 over MMP-1. Insertion of an ether linkage between the two aryl rings led to an increase in selectivity over MMP-1. Selectivity was further improved after replacement of the barbituric acid group by a phenyl. Docking in MMP-2 and analysis of GRID/CPCA differential plots provide an explanation for the selectivity differences sum-

marized in Table 3. Our results suggest that replacing the ether by a sulfone mainly affects the electron density on the biaryl system while leaving the binding mode unchanged (Figure 5H, left panel). More precisely, the only PC2 differential plot showing variations around the sulfone group is the one obtained for the N1 probe. We assume that this electronic effect affects more strongly the MMP-1 activity (Table 3). In other words, the change in electron density on the biaryl ring makes up for the steric hindrance resulting from the binding of a large substituent to the shallow S1′ subpocket of MMP-1. The subsequent introduction of an ether linker between the two phenyls is sufficient to once again take advantage of the size difference between the S1′ subpocket of MMP-1 and -2 (Figure 5H, middle panel) and hence to improve the selectivity of the sulfones (Table 3). As illustrated in the right panel of Figure 5H, the replacement of the barbituric acid group by a phenyl alters the S1′ binding group and hence exploits the difference in size of the S1′ pocket. Again, this interpretation is consistent with the chemometric analysis, which has highlighted limited opportunities for selective interactions within the S1 pocket.

2.8.9. 2-Oxoimidazolidine. In another case, exploitation of the size difference between the S1′ pocket of MMP-3 and MMP-13 was sufficient to achieve within a class of 2-oxoimidazolidine inhibitors, a selectivity of up to 460-fold for MMP-13 over MMP-3.[90] When docked in MMP-3, the S1′ binding group of compound **14** (Figure 5I, IC$_{50}$ of 1380 and 3 nM for MMP-3 and -13) overlaps with positive contours of the PC2 differential CPCA plot obtained for the GRID C3 probe (Figure 5I, right panel). In PC2, these positive contours highlight regions of the S1′ pocket where selectivity for MMP-13 over MMP-3 can be increased.

3. Conclusion

The present analysis indicates possibilities for the design of selective MMP inhibitors, as the quest for selectivity still constitutes one of the main challenges in the search for successful clinical candidates. On the basis of a large data set containing 53 MMP X-ray structures and one TACE X-ray structure plus three homology models, we systematically explored differences in aligned MMP binding sites. To this end, two methods to describe MMP binding sites based on force field interaction energies (GRID) or knowledge-based statistical potentials (DrugScore) were investigated. A consensus principal component analysis (CPCA) for all the MMP binding sites and the six subpockets was performed. We found that both approaches, GRID/CPCA and DrugScore/CPCA, capture similar information with respect to the discrimination between different MMPs while the relative importance of the probes varies between GRID and DrugScore. For DrugScore, the nonpolar probes contribute predominantly to the CPCA models, while for GRID, there are pockets where a polar probe is equally important.

Some general trends for inhibitor design can be derived from this study. Corresponding substituents in S1′ discriminate MMP-3 from MMP-8 on one hand and MMP-1 and -7 on the other hand, while other MMPs occupy the space between the MMP-3 and -8 clusters. While nonpolar probes are important, polar interactions can be exploited to achieve selectivity in some cases. A poor separation is present in S2′ with one exception, namely, the possibility for the DrugScore Cl probe to discriminate MMP-14 from other MMPs. S3′ allows for separation of the collagenases and MMP-2 from other MMP subtypes based on contributions from both polar and nonpolar probes. In S1, a poor separation of the MMPs is found, while MMP-16 is slightly

separated from the others. However, the combined interpretation with inhibitor data consistently highlights possibilities for selectivity in the area, especially when linking S1 and S2 in some inhibitors. The S2 pocket allows for separation of human collagenases, gelatinases, MMP-11, -12, and -16 versus MMP-3, -7, -10, -14 and mouse MMP-13 with contributions of nonpolar interactions. Finally, some substituents in S3 separate MMP-1 -, 8, -11, and -14 from all the others. The GRID probes exhibit roughly the same contributions, while for DrugScore the hydrophobic probes are more important. These models allow for the following ranking of the MMP subpockets based on the possibility of achieving selective interactions: S1′ > S2, S3, S3′ > S1, S2′. This ranking is the same using either GRID or DrugScore.

The chemical interpretation of these models for individual pockets in combination with inhibitor selectivity profiles and binding modes from X-ray structure analysis or docking results in the consistent identification of selectivity regions for discrimination of MMP family members. In agreement with previous data, the S1′ pocket appears as the primary site of intervention for obtaining selectivity. Binding of additional groups to the other subpockets can also contribute to selective inhibition of a particular MMP while sparing the others. These analyses have identified the regions offering opportunities for selective interactions with different MMPs. Our results also highlight the importance of hydrophobic, steric, and nonpolar interactions for achieving selectivity.

Collectively these analyses define the three-dimensional structural biology space for this target family and allow the analysis of inhibitor binding modes in order to rationalize experimentally observed MMP selectivity profiles. A consistent view on selectivity from the perspective of proteins and ligands emerges. Results from these analyses suggest that there is no unique solution to this problem exploring only one subpocket, although selectivity toward MMP-13 has been obtained by only exploiting flexibility of the loop at the bottom of the S1′ pocket.[91] Future publications on MMP inhibitors might reveal whether this latter example is unique or not.

4. Methods

4.1. General. All modeling studies were done using the program SYBYL[92] on SGI workstations. Docking and protein superposition steps were automated using scripts in PERL and SPL (SYBYL Programming Language). All energy calculations were based on the MMFF94s force field[93] using MMFF94 charges. Conformations of ligands and complexes were minimized using quasi Newton−Raphson or conjugate gradient procedures.

4.2. Crystallographic Data. The 1.7 Å X-ray crystal structure of MMP-8 in complex with compound **4** (Chart 1, PDB code 1BZS)[58] was used to search the protein−ligand database Reli-Base+[36,67,94] for high-resolution structures (<3.0 Å) sharing >40% sequence identity, resulting in 55 hits: 54 MMP X-ray structures and one TACE (tumor necrosis factorα converting enzyme) X-ray structure, as summarized in Table 1. Multiple binding sites per subfamily were considered to account for conformation variations in particular subpockets.

4.3. Homology Modeling. Homology models of the MMP-10 and -16 catalytic domains were retrieved from Wayne State University Web site.[54,95] MMP-10 and -16 share 85% and 68% sequence identity with MMP-3 and -14, respectively. The homology model for the MMP-9 catalytic domain was built using the program MOE.[96] To this end, the X-ray crystal structure of MMP-2 (PDB code 1QIB[97]) revealing the highest sequence identity to MMP-9 (64%) was used as a template based on the sequence alignment to all members of the MMP family in the MOE protein database. Homology models based on more than 50% sequence identity to their template are generally considered as high-accuracy models.[98]

Their accuracy is comparable to the accuracy of low-resolution X-ray structures. The errors are mostly mistakes in side chain packing, small shifts or distortion of the core main chain regions, and larger errors in loops. However, errors in the biologically important regions tend to be lower because of their high conservation compared to the rest of the structure. Homology models have been previously used to rationalize structure−activity relationships and selectivity of ligands against homologous proteins. We refer the interested readers to a recent review on homology modeling.[98]

The MOE coarse minimization option was used for final refinement, resulting in 10 models differing in side chain or loop conformations. These models were analyzed with tools in MOE (Homology Modelling) and SYBYL (ProTable). The MMP-9 model with the lowest number of alerts was retained. In addition, the models for MMP-10 and -16 plus crystal structures with a resolution greater than 2.5 Å were checked and considered as satisfactory.

4.4. 3D Structure Alignment. A global unbiased alignment based on secondary structures plus structurally conserved regions (SCRs) was carried out for the 57 MMP structures (54 crystal structures and 3 homology models). To start with, the SYBYL implementation of Composer[99] was run to align the MMP sequences to the template (PDB code 1BZS). The identified seed residues served as a basis for 3D structural alignment, leading to the identification of structurally conserved regions among the entire protein ensemble. In two iterations, residues with greater than 2 standard deviations were rejected, leading to an optimized alignment with acceptable superposition of SCRs and cavities for all the structures but the full-length MMP-2 (PDB code 1CK7), which was subsequently discarded. The alignment of the 56 MMP structures considered for the subsequent analyses is shown in Figure 1B. To align the less similar protein TACE to the ensemble of MMP structures, the global alignment procedure described above was performed and followed by a local alignment of the SCRs lining the binding site, which also resulted in an acceptable superposition of the SCRs and cavities, particularly on the right-hand side.

4.5. GRID Interaction Fields. After removal of cofactors, counterions, ligands, and structural water, the 57 aligned structures were checked and corrected for missing parts without being neutralized. Hydrogen atoms were added to the structures using the program GRIN. All GRID[16,17] calculations were carried out in a 34 Å × 43 Å × 42 Å box with a 1 Å grid size enclosing the catalytic domains of all structures. During the GRID calculations, all amino acid side chains were kept rigid (GRID directive MOVE = 0). Instead, protein flexibility was taken into account by considering all the available PDB entries for a given MMP subtype. The main advantage of this approach is that it accounts for conformational changes induced by inhibitor binding. The following probes were found to be informative[28] to identify binding site regions conferring selectivity: hydrophobic (DRY), methyl (C3) for steric interactions, amide nitrogen (N1, hydrogen bond donor), carbonyl oxygen (O, hydrogen bond acceptor), and phenolic oxygen (OH, hydrogen bond acceptor and donor). The data from GRID molecular interaction fields were organized as described previously[24,28] in a vector containing x GRID probes × n GRID interaction points for each protein structure as row.

4.6. DrugScore Interaction Fields. The 3D structures were additionally characterized using knowledge-based potentials in DrugScore, version 1.2.[33,34] The identical grid box encompassing all MMP catalytic sites with a 1.0 Å grid spacing served to evaluate the propensity of interactions between each structure and the following six SYBYL atom types: sp³ carbon (C.3), sp² oxygen (O.2), amide nitrogen (N.am), sp² carbon (C.2), sp³ oxygen (O.3), and chlorine (Cl). All data were organized similarly to GRID derived molecular interaction fields.

4.7. Consensus Principal Component Analysis (CPCA). The individual **X** matrices from GRID or DrugScore were analyzed using PCA[18] and Consensus PCA[24,25] implemented in GOLPE.[64,100] Only attractive protein−ligand interactions from GRID (negative energy values) and DrugScore (propensity greater than 70%) were retained. Two- and three-level variables and columns with SD less

than 0.01 kcal mol^{-1} were rejected, and block scaling (BUW) was applied to normalize the importance of all probes in the final models.[24]

Consensus PCA (CPCA[24,25]) is a PCA variation to analyze data organized in blocks. Here, each block contains the molecular interaction field (MIF) between a GRID/DrugScore probe and each binding site. The aim of CPCA is to capture both the global structure of the MIF matrix, as from a "global" PCA, and the structure of each block through PCAs for each sub-block. Thus, CPCA provides global scores and loadings representing the "consensus" of all probes and provides block scores and loadings expressing the "point of view" of each probe.

This analysis was focused on interactions within 4 Å around the consensus ligand binding region for the entire target family landscape and subsequently to each subpocket using the cutout functionality in GOLPE, version 4.5. To define a pocket, the amino acids within 8.0 Å (S1′) or 4.0 Å (other pockets) of an inhibitor fragment bound to a given pocket in a particular crystal structure were used.

4.8. CPCA Model Analysis Strategy. CPCA models were analyzed using score plots, which unveiled clustering of similar MMP binding sites favorably interacting with particular probes. It should be noted that any grouping of targets is based on similar protein–ligand 3D interaction patterns and not on 1D sequence similarity. Furthermore, the GOLPE active plots[64] enabled us to focus on relative differences between target binding site interactions, which allows for a separation of 3D binding sites.

4.9. Ligand Analysis. For manual docking of candidate molecules, X-ray crystal structures for MMP-2, MMP-3, and MMP-8 were used (PDB codes 1QIB, 1CAQ, 1BZS). Compounds were manually built using the most similar inhibitor X-ray structure as template. The resulting protein–ligand complexes were docked into the corresponding MMP binding site and minimized treating all inhibitor atoms plus selected protein residues within a sphere of 5 Å around the ligand as flexible using QXP.[101] The remaining protein was only used to compute nonbonded iteractions. Other compounds were manually built, superimposed onto this template, and minimized under identical conditions. The ligand binding modes were analyzed using GOLPE active plots[64] to investigate relative differences between MMP binding site interactions to understand experimental selectivity differences.

References

(1) Klebe, G., Ed. *Virtual Screening: An Alternative or Complement to High Throughput Screening*; Kluwer/Escom: Dordrecht, The Netherlands, 2000.

(2) Schneider, G.; Böhm, H.-J. Virtual screening and fast automated docking methods. *Drug Discovery Today* **2002**, *7*, 64–70.

(3) Böhm, H.-J., Schneider, G., Eds. *Virtual Screening for Bioactive Molecules*; Wiley-VCH: Weinheim, Germany, 2000.

(4) Klebe, G. Recent developments in structure-based drug design. *J. Mol. Med.* **2000**, *78*, 269–281.

(5) Murcko, M. A.; Caron, P. R.; Charifson, P. S. Structure-based drug design. *Annu. Rep. Med. Chem.* **1999**, *34*, 297–306.

(6) Gane, P. J.; Dean, P. M. Recent advances in structure-based rational drug design. *Curr. Opin. Struct. Biol.* **2000**, *10*, 401–404.

(7) Kubinyi, H. Structure-based design of enzyme inhibitors and receptor ligands. *Curr. Opin. Drug Discovery Dev.* **1998**, *1*, 4–15.

(8) Böhm, H.-J.; Stahl, M. Structure-based library design: molecular modelling merges with combinatorial chemistry. *Curr. Opin. Chem. Biol.* **2000**, *4*, 283–286.

(9) Kornberg, A. The two cultures. Chemistry and biology. *Biochemistry* **1987**, *26*, 6888–6891.

(10) Wess, G.; Urmann, M.; Sickenberger, B. Medicinal chemistry: challenges and opportunities. *Angew. Chem., Int. Ed.* **2001**, *40*, 3341–3350.

(11) Caron, P. R.; Mullican, M. D.; Mashal, R. D.; Wilson, K. P.; Su, M. S.; Murcko, M. A. Chemogenomic approaches to drug discovery. *Curr. Opin. Chem. Biol.* **2001**, *5*, 464–470.

(12) Lehman, J.; Baxter, A.; Brown, D.; Connolly, P.; Geysin, M.; Hayes, M.; Howard, R.; Knowles, J.; Lee, M.; Lyall, A.; et al. Systematization of research. *Nature* **1996**, *384* (Suppl. 7), 5.

(13) Bemis, G. W.; Murcko, M. A. The properties of known drugs. 1. Molecular frameworks. *J. Med. Chem.* **1996**, *39*, 2887–2893.

(14) Ajay; Bemis, G. W.; Murcko, M. A. Designing libraries with CNS activity. *J. Med. Chem.* **1999**, *42*, 4942–4951.

(15) Blundell, T. L.; Jhoti, H.; Abell, C. High-throughput crystallography for lead discovery in drug design. *Nat. Rev.* **2002**, *1*, 45–54.

(16) (a) Goodford, P. J. A computational procedure for determining energetically favorable binding sites on biologically important macromolecules. *J. Med. Chem.* **1985**, *28*, 849–857. (b) Boobbyer, D. N. A.; Goodford, P. J.; McWhinnie, P. M.; Wade, R. C. New hydrogen-bond potentials for use in determining energetically favorable binding sites on molecules of known structure. *J. Med. Chem.* **1989**, *32*, 1083–1094. (c) Wade, R. C.; Clerk, K. J.; Goodford, P. J. Further development of hydrogen bond functions for use in determining energetically favorable binding sites on molecules of known structure. 1. Ligand probe groups with the ability to form two hydrogen bonds. *J. Med. Chem.* **1993**, *36*, 140–147. (d) Wade, R. C.; Goodford, P. J. Further development of hydrogen bond functions for use in determining energetically favorable binding sites on molecules of known structure. 2. Ligand probe groups with the ability to form more than two hydrogen bonds. *J. Med. Chem.* **1993**, *36*, 148–156.

(17) *GRID*, version 19; Molecular Discovery Ltd. (West Way House, Elms Parade): Oxford, U.K., 2001.

(18) (a) Wold, S.; Esbensen, K.; Geladi, P. Principal component analysis. *Chemom. Intell. Lab. Syst.* **1987**, *2*, 37–52. (b) Dillon, W. R.; Goldstein, M. *Multivariate Analysis: Methods and Applications*; Wiley: New York, 1984. (c) Malinowski, E. R.; Howery, D. G. *Factor Analysis in Chemistry*; Wiley: New York, 1980. (d) Stahle, L.; Wold, S. Multivariate Data Analysis and Experimental Design in Biomedical Research. In *Progress in Medicinal Chemistry* Ellis, G. P., West, G. B., Eds.; Elsevier: Amsterdam, The Netherlands, 1988; pp 292–338. (e) Wold, S.; Albano, C.; Dunn, W. J., III; Edlund, U.; Esbensen, K.; Geladi, P.; Hellberg, S.; Johanson, E.; Lindberg, W.; Sjöström, M. Multivariate Data Analysis in Chemistry. In *Chemometrics: Mathematics and Statistics in Chemistry*; Kowalski, B. R., Ed.; NATO, ISI Series C 138; D. Reidel Publ. Co.; Dordrecht, The Netherlands, 1984; pp 17–96.

(19) Cruciani, G.; Goodford, P. J. A search for specificity in DNA–drug interactions. *J. Mol. Graphics* **1994**, *12*, 116–129.

(20) Pastor, M.; Cruciani, G. A novel strategy for improving ligand selectivity in receptor-based drug design. *J. Med. Chem.* **1995**, *38*, 4637–4647.

(21) Matter, H.; Schwab, W. Affinity and selectivity of matrix metalloproteinase inhibitors: a chemometrical study from the perspective of ligands and proteins. *J. Med. Chem.* **1999**, *42*, 4506–4523.

(22) Matter, H.; Schwab, W. A View on Affinity and Selectivity of Nonpeptidic Matrix Metalloproteinase Inhibitors from the Perspective of Ligands and Target. In *Molecular Modeling and Prediction of Bioactivity*; Gundertofte, K., Jørgensen, F. S., Eds.; Kluwer: New York, 2000; pp 123–128.

(23) Filipponi, E.; Cecchetti, V.; Tabarrini, O.; Bonelli, D.; Fravolini, A. Chemometric rationalization of the structural and physicochemical basis for selective cyclooxygenase-2 inhibition: toward more specific ligands. *J. Comput.-Aided Mol. Des.* **2000**, *14*, 277–291.

(24) Kastenholz, M. A.; Pastor, M.; Cruciani, G.; Haaksma, E. E. J.; Fox, T. GRID/CPCA: a new computational tool to design selective ligands. *J. Med. Chem.* **2000**, *43*, 3033–3044.

(25) Westerhuis, J. A.; Kourti, T.; Macgregor, J. F. Analysis of multiblock and hierarchical PCA and PLS models. *J. Chemom.* **1998**, *12*, 301–321.

(26) Matter, H.; Defossa, E.; Heinelt, U.; Naumann, T.; Schreuder, H.; Wildgoose, P. Combining Structure-based Design and 3D-QSAR towards the Discovery of Non-chiral, Potent and Selective Factor Xa Inhibitors. In *Rational Approaches to Drug Design*, Proceedings of the 13th European Symposium on Quantitative Structure–Activity Relationships; Höltje, H.-D., Sippl, W., Eds.; Prous Science: Barcelona, Spain, 2001; pp 177–185.

(27) Ridderström, M.; Zamora, I.; Fjellström, O.; Andersson, T. B. Analysis of selective regions in the active sites of human cytochromes P450, 2C8, 2C9, 2C18, and 2C19 homology models using GRID/CPCA. *J. Med. Chem.* **2001**, *44*, 4072–4081.

(28) Naumann, T.; Matter, H. Structural classification of protein kinases using 3D molecular interaction field analysis of their ligand binding sites: target family landscapes. *J. Med. Chem.* **2002**, *45*, 2366−2378.

(29) Terp, G. E.; Cruciani, G.; Christensen, I. T.; Jorgensen, F. S. Structural differences of matrix metalloproteinases with potential implications for inhibitor selectivity examined by the GRID/CPCA approach. *J. Med. Chem.* **2002**, *45*, 2675−2684.

(30) Reiter, L. A.; Rizzi, J. P.; Pandit, J.; Lasut, M. J.; McGahee, S. M.; Parikh, V. D.; Blake, J. F.; Danel, D. E.; Laird, E. R.; Lopez-Anaya, A.; Lopresti-Morrow, L. L.; Mansour, M. N.; Martinelli, G. C.; Mitchell, P. G.; Owens, B. S.; Pauly, T. A.; Reeves, L. M.; Schulte, G. K.; Yocum, S. A. Inhibition of MMP-1 and MMP-13 with phosphinic acids that exploit binding in the S2 pocket. *Bioorg. Med. Chem. Lett.* **1999**, *9*, 127−132.

(31) Finzel, B. C.; Baldwin, E. T.; Bryant, G. L., Jr.; Hess, G. F.; Wilks, J. W.; Trepod, C. M.; Mott, J. E.; Marshall, V. P.; Petzold, G. L.; Poorman, R. A.; O'Sullivan, T J.; Schostarez, H. J.; Mitchell, M. A. Structural characterizations of nonpeptidic thiadiazole inhibitors of matrix metalloproteinases reveal the basis for stromelysin selectivity. *Protein Sci.* **1998**, *7*, 2118−2126.

(32) Lukacova, V.; Zhang, Y.; Mackov, M.; Baricic, P.; Raha, S.; Calva, J. A.; Balaz, S. Similarity of binding sites of human matrix metalloproteinases. *J. Biol. Chem.* **2004**, *279*, 14194−14200.

(33) Gohlke, H.; Hendlich, M.; Klebe, G. Knowledge-based scoring function to predict protein−ligand interactions. *J. Mol. Biol.* **2000**, *295*, 337−356.

(34) Gohlke, H.; Hendlich, M.; Klebe, G. Predicting binding modes, binding affinities and "hot spots" for protein−ligand complexes using a knowledge-based scoring function. *Perspect. Drug Discovery Des.* **2000**, *20*, 115−144.

(35) (a) RCSB Protein Data Bank, from the Research Collaboratory for Structural Bioinformatics: http://www.rcsb.org/pdb/index.html. (b) Berman, H. M.; Westbrook, J.; Feng, Z.; Gilliland, G.; Bhat, T. N.; Weissig, I.; Shindyalov, I. N.; Bourne, P. E. The protein data bank. *Nucleic Acids Res.* **2000**, *28*, 235−242.

(36) Hendlich, M. Databases for protein−ligand complexes. *Acta Crystallogr., Sect. D* **1998**, 54, 1178−1182.

(37) Gohlke, H.; Klebe, G. Statistical potentials and scoring functions applied to protein−ligand binding. *Curr. Opin. Struct. Biol.* **2001**, *11*, 231−235.

(38) (a) Mügge, I.; Martin, Y. C. A general and fast scoring function for protein−ligand interactions: a simplified potential approach. *J. Med. Chem.* **1999**, *42*, 791−804. (b) Mügge, I.; Martin, Y. C.; Hajduk, P. J.; Fesik, S. W. Evaluation of PMF scoring in docking weak ligands to the FK506 binding protein. *J. Med. Chem.* **1999**, *42*, 2498−2503.

(39) (a) Mitchell, J. B. O.; Laskowski, R. A.; Alex, A.; Thornton, J. M. BLEEP−Potential of mean force describing protein−ligand interactions. I. Generating potentials. *J. Comput. Chem.* **1999**, *20*, 1165−1176. (b) Mitchell, J. B. O.; Laskowski, R. A.; Alex, A.; Forster, M. J.; Thornton, J. M. BLEEP−Potential of mean force describing protein−ligand interactions. II. Calculation of binding energies and comparison with experimental data. *J. Comput. Chem.* **1999**, *20*, 1177−1185.

(40) Sotriffer, C. A.; Gohlke, H.; Klebe, G. Docking into knowledge-based potential fields: a comparative evaluation of DrugScore. *J. Med. Chem.* **2002**, *45*, 1967−1970.

(41) Matter, H.; Schudok, M. Recent advances in the design of matrix metalloproteinase inhibitors. *Curr. Opin. Drug Discovery Dev.* **2004**, *7*, 513−535.

(42) (a) Woessner, J. F., Jr. Matrix metalloproteinases and their inhibitors in connective tissue remodeling. *FASEB J.* **1991**, *5*, 2145−2154. (b) Birkedal-Hansen, H.; Moore, W. G. I.; Bodden, M. K.; Windsor, L. J.; Birkedal-Hansen, B.; DeCarlo, A.; Engler, J. A. Matrix metalloproteinases: a review. *Crit. Rev. Oral Biol. Med.* **1993**, *4*, 197−250. (c) Murphy, G.; Docherty, A. J. P. The matrix metalloproteinases and their inhibitors. *Am. J. Respir. Cell Mol. Biol.* **1992**, *7*, 120−125. (d) Matrisian, L. M. Metalloproteinases and their inhibitors in matrix remodeling. *Trends Genet.* **1990**, *6*, 121−125.

(43) Skiles, J. W.; Gonnella, N. C.; Jeng, A. Y. The design, structure, and therapeutic application of matrix metalloproteinase inhibitors. *Curr. Med. Chem.* **2001**, *8*, 425−474.

(44) (a) Goldring, M. B. Degradation of Articular Cartilage in Culture: Regulatory Factors. In *Joint Cartilage Degradation*; Woessner, J. F., Howell, D. S., Eds.; Dekker: New York 1993; pp 281−346. (b) Willenbrock, F.; Murphy, G. Structure−function relationships in the tissue inhibitors of metalloproteinases. *Am. J. Respir. Crit. Care Med.* **1994**, *150*, 5165−5170. (c) Murphy, G.; Willenbrock, F. Tissue inhibitors of matrix metalloendopeptidases. *Methods Enzymol.* **1995**, *248*, 496−510.

(45) Kleiner, D. E.; Stetler-Stevenson, W. G. Matrix metalloproteinases and metastasis. *Cancer Chemother. Pharmacol.* **1999**, *43* (Suppl.), S42−S51.

(46) Lohmander, L. S.; Hoerrner, L. A.; Lark, M. W. Metalloproteinases, tissue inhibitor, and proteoglycan fragments in knee synovial fluid in human osteoarthritis. *Arthritis Rheum.* **1993**, *36*, 181−189.

(47) Murphy, G.; Hembry, R. M. Proteinases in rheumatoid arthritis. *J. Rheumatol.* **1992**, *19*, 61−64.

(48) Peress, N.; Perillo, E.; Zucker, S. Localization of tissue inhibitor of matrix metalloproteinases in Alzheimer's disease and normal brain. *J. Neuropathol. Exp. Neurol.* **1995**, *54*, 16−22.

(49) Bode, W.; Reinemer, P.; Huber, R.; Kleine, T.; Schnierer, S.; Tschesche, H. The X-ray crystal structure of the catalytic domain of human neutrophil collagenase inhibited by a substrate analogue reveals the essentials for catalysis and specificity. *EMBO J.* **1994**, *13*, 1263−1269.

(50) Murphy, G. J.; Murphy, G.; Reynolds, J. J. The origin of matrix metalloproteinases and their familial relationships. *FEBS Lett.* **1991**, *89*, 4−7.

(51) Pendas, A. M.; Knauper, V.; Puente, X. S.; Llano, E.; Mattei, M. G.; Apte, S.; Murphy, G.; Lopez Otin, C. Identification and characterization of a novel human matrix metalloproteinase with unique structural features, chromosomal location, and tissue distribution. *J. Biol. Chem.* **1997**, *272*, 4281−4286.

(52) (a) Borkakoti, N. Structural studies on matrix metalloproteinases. *J. Mol. Med.* **2000**, *78*, 261−268. (b) Borkakoti, N. The structural basis of matrix metalloproteinase inhibition. *Curr. Opin. Drug Discovery* **1999**, *2*, 449−462.

(53) Li, J.; Brick, P.; O'Hare, M. C.; Skarzynski, T.; Lloyd, L. F.; Curry, V. A.; Clark, I. M.; Bigg, H. F.; Hazleman, B. L.; Cawston, T. E.; Blow, D. M. Structure of the full length porcine synovial collagenase reveals a C-terminal domain containing a calcium-linked, four bladed beta propeller. *Structure* **1995**, *3*, 541−549.

(54) Massova, I.: Kotra, L. P.; Fridman, R.; Mobashery, S. Matrix metalloproteinases: structures, evolution and diversification. *FASEB J.* **1998**, *12*, 1075−1095.

(55) Frye, S. V. Structure−activity relationship homology (SARAH): a conceptual framework for drug discovery in the genomic area. *Chem. Biol.* **1999**, *6*, R3−R7.

(56) Stams, T.; Spurlino, J. C.; Smith, D. L.; Wahl, R. C.; Ho, T. F.; Qoronfleh, M. W.; Banks, T. M.; Rubin, B. Structure of human neutrophil collagenase reveals large S1′ specificity pocket. *Nat. Struct. Biol.* **1994**, *1*, 119−23.

(57) Welch, A. R.; Holman, C. M.; Huber, M.; Brenner, M. C.; Browner, M. F.; Van Wart, H. E. Understanding the P1′ specificity of the matrix metalloproteinases: effect of S1′ pocket mutations in matrilysin and stromelysin-1. *Biochemistry* **1996**, *35*, 10103−10109.

(58) Matter, H.; Schwab, W.; Barbier, D.; Billen, G.; Haase, B.; Neises, B.; Schudok, M.; Thorwart, W.; Schreuder, H.; Brachvogel, V.; Loenze, P.; Weithmann, K. U. Quantitative structure−activity relationship of human neutrophil collagenase (MMP-8) inhibitors using comparative molecular field analysis and X-ray structure analysis. *J. Med. Chem.* **1999**, *42*, 1908−1920.

(59) Browner, M. F.; Smith, W. W.; Castelhano, A. L. Crystal structures of matrilysin-inhibitor complexes. *Biochemistry* **1995**, *34*, 6602−10.

(60) Lovejoy, B.; Welch, A. R.; Carr, S.; Luong, C.; Broka, C.; Hendricks, R. T.; Campbell, J. A.; Walker, K. A. M.; Martin, R.; Van Wart, H.; Browner, M. F. Crystal structures of MMP-1 and -13 reveal the structural basis for selectivity of collagenase inhibitors. *Nat. Struct. Biol.* **1999**, *6*, 217−221.

(61) Moy, F. J.; Chanda, P. K.; Chen, J.; Cosmi, S.; Edris, W.; Levin, J. I.; Rush, T. S.; Wilhelm, J.; Powers, R. Impact of mobility on structure-based drug design for the MMPs. *J. Am. Chem. Soc.* **2002**, *124*, 12658−12659.

(62) Källblad, P.; Todorov, N. P.; Willems, H. M. G.; Alberts, I. L. Receptor flexibility in the in silico screening of reagents in the S1′ pocket of human collagenases. *J. Med. Chem.* **2004**, *47*, 2761−2767.

(63) Steele, D. L.; El-Kabbani, O.; Dunten, P.; Windsor, L. J.; Kammlott, R. U.; Crowther, R. L.; Michoud, C.; Engler, J. A.; Birktoft, J. J. Expression, characterization and structure determination of an active site mutant (Glu202-Gln) of mini-stromelysin-1. *Protein Eng.* **2000**, *13*, 397−405.

(64) *GOLPE*, version 4.5.; Multivariate Infometric Analysis, Srl (Viale die Castagni, 16): Perugia, Italy, 1999.

(65) Nar, H.; Werle, K.; Bauer, M. M. T.; Dollinger, H.; Jung, B. Crystal structure of human macrophage elastase (MMP-12) in complex with a hydroxamic acid inhibitor. *J. Mol. Biol.* **2001**, *312*, 743−751.

(66) Matter, H.; Will, D. W.; Nazaré, M.; Schreuder, H.; Laux, V.; Wehner, V. Structural requirements for factor Xa inhibition by 3-oxybenzamides with neutral P1 substituents: combining X-ray crystallography, 3D-QSAR and tailored scoring functions. *J. Med. Chem.* **2005**, *48*, 3920−3312.

(67) Bergner, A.; Günther, J.; Hendlich, M.; Klebe, G.; Verdonk, M. Use of Relibase for retrieving complex three-dimensional interaction patterns including crystallographic packing effects. *Biopolymers* **2002**, *61*, 99−110.

(68) Borkakoti, N.; Winkler, F. K.; Williams, D. H.; D'Arcy, A.; Broadhurst, M. J.; Brown, P. A.; Johnson, W. H.; Murray, E. J. Structure of the catalytic domain of human fibroblast collagenase complexed with an inhibitor. *Nat. Struct. Biol.* **1994**, *1*, 106−110.

(69) Natchus, M. G.; Cheng, M.; Wahl, C. T.; Pikul, S.; Almstead, N. G.; Bradley, R. S.; Taiwo, Y. O.; Mieling, G. E.; Dunaway, C. M.; Snider, C. E.; Mciver, J. M.; Barnett, B. L.; Mcphail, S. J.; Anastasio, M. B.; De, B. Design and synthesis of conformationally-constrained MMP inhibitors. *Bioorg. Med. Chem. Lett.* **1998**, *8*, 2077−2080.

(70) Babine, R. E.; Bender, S. L. Molecular recognition of protein−ligand complexes: applications to drug design. *Chem. Rev.* **1997**, *97*, 1359−1472.

(71) Stockman, B. J.; Waldon, D. J.; Gates, J. A.; Scahill, T. A.; Kloosterman, D. A.; Mizsak, S. A.; Jacobsen, E. J.; Belonga, K. L.; Mitchell, M. A.; Mao, B.; Petke, J. D.; Goodman, L.; Powers, E. A.; Ledbetter, S. R.; Kaytes, P. S.; Vogeli, G.; Marshall, V. P.; Petzold, G. L.; Poorman, R. A. Solution structures of stromelysin complexed to thiadiazole. *Protein Sci.* **1998**, *7*, 2281−2286.

(72) Botos, I.; Meyer, E.; Swanson, S. M.; Lemaitre, V.; Eeckhout, Y.; Meyer, E. F. Structure of recombinant mouse collagenase-3 (MMP-13). *J. Mol. Biol.* **1999**, *292*, 837−844.

(73) Whittaker, M.; Floyd, C. D.; Brown, P.; Gearing, A. J. H. Design and therapeutic application of matrix metalloproteinase inhibitors. *Chem. Rev.* **1999**, *99*, 2735−2776.

(74) Brown, S.; Meroueh, S. O.; Fridman, R.; Mobashery, S. Quest for selectivity in inhibition of matrix metalloproteinases. *Curr. Top. Med. Chem.* **2004**, *4*, 1227−1238.

(75) Coussens, L. M.; Fingleton, B.; Matrisian, L. M. Matrix metalloproteinase inhibitors and cancer: trials and tribulations. *Science* **2002**, *295*, 2387−2392.

(76) Hanessian, S.; Bourbouz, S.; Boudon, A.; Tucker, G. C.; Peyroulan, D.; Picking the S1, S1′ and S2′ pockets of matrix metalloproteinases. A niche for potent acyclic sulfonamide inhibitors. *Bioorg. Med. Chem. Lett.* **1999**, *9*, 1691−1696.

(77) Hanessian, S.; Moitessier, N.; Gauchet, C.; Viau, M. *N*-Aryl sulfonyl homocysteine hydroxamate inhibitors of matrix metalloproteinases: further probing of the S1, S1′, and S2′ pockets. *J. Med. Chem.* **2001**, *44*, 3066−3073.

(78) Hanessian, S.; MacKay, D. B.; Moitessier, N. Design and synthesis of matrix metalloproteinase inhibitors guided by molecular modeling. Picking the S1 pocket by conformationally constrained inhibitors. *J. Med. Chem.* **2001**, *44*, 3074−3082.

(79) Vassiliou, S.; Mucha, A.; Cuniasse, P.; Georgiadis, D.; Lucet-Levannier, K.; Beau, F.; Kannan, R.; Murphy, G.; Knäuper, V.; Rio, M. C.; Basset, P.; Yiotakis, A.; Dive, V. Phosphinic pseudo-tripeptides as potent inhibitors of matrix metalloproteinases: a structure−activity study. *J. Med. Chem.* **1999**, *42*, 2610−2620.

(80) Gall, A. L.; Ruff, M.; Kannan, R.; Cuniasse, P.; Yiotakis, A.; Dive, V.; Rio, M. C.; Basset, P.; Moras, D. Crystal structure of the stromelysin-3 (MMP-11) catalytic domain complexed with a phosphinic inhibitor mimicking the transition state. *J. Mol. Biol.* **2001**, *307*, 577−586.

(81) Mucha, A.; Cuniasse, P.; Kannan, R.; Beau, F.; Yiotakis, A.; Basset, P.; Dive, V. Membrane type-1 matrix metalloprotease and stromelysin-3 cleave more efficiently synthetic substrates containing unusual amino acids in their P1′ positions. *J. Biol. Chem.* **1998**, *273*, 2763−2768.

(82) Matter, H.; Schudok, M.; Schwab, W.; Thorwart, W.; Barbier, D.; Billen, G.; Haase, B.; Neises, B.; Weithmann, K. U.; Wollmann, T. Tetrahydroisoquoinoline-3-carboxylate based matrix metalloproteinase inhibitors: design, synthesis and structure−activity relationship. *Bioorg. Med. Chem.* **2002**, *10*, 3529−3544.

(83) Cherney, R. J.; Wang, L.; Meyer, D. T.; Xue, C. B.; Wasserman, Z. R.; Hardman, K. D.; Welch, P. K.; Covington, M. B.; Copeland, R. A.; Arner, E. C.; DeGrado, W. F.; Decicco, C. P. Macrocyclic amino carboxylates as selective MMP-8 inhibitors. *J. Med. Chem.* **1998**, *41*, 1749−1751.

(84) Cherney, R. J.; Decicco, C. P.; Nelson, C. R.; Wan, L.; Meyer, D. T.; Hardman, K. D.; Copeland, R. A.; Arner, E. C. Potent carboxylate inhibitors of stromelysin containing P2′ piperazic acids and P1′ biaryl moieties. *Bioorg. Med. Chem. Lett.* **1997**, *7*, 1757−1762.

(85) Betz, M.; Huxley, P.; Davies, S.; Mushtaq, Y.; Pieper, M.; Tschesche, H.; Bode, W.; Gomis-Ruth, F. 1.8-Å crystal structure of the catalytic domain of human neutrophil collagenase (matrix metalloproteinase-8) complexed with a peptidomimetic hydroxamate primed-side inhibitor with a distinct selectivity profile. *Eur. J. Biochem.* **1997**, *247*, 356−363.

(86) Tamura, Y.; Watanabe, F., Nakatani, T.; Yasui, K.; Fuji, M.; Komurasaki, T.; Tsuzuki, H.; Maekawa, R.; Yoshioka, T.; Kawada, K.; Sugita, K.; Ohtani, M. Highly selective and orally active inhibitors of type IV collagenase (MMP-9 and MMP-2): *N*-sulfonylamino acid derivatives. *J. Med. Chem.* **1998**, *41*, 640−649.

(87) Foley, L. H.; Palermo, R.; Dunten, P.; Wang, P. Novel 5,5-disubstitutedpyrimidine-2,4,6-triones as selective MMP inhibitors. *Bioorg. Med. Chem. Lett.* **2001**, *11*, 969−972.

(88) Dunten, P.; Kammlott, U.; Crowther, R.; Levin, W.; Foley, L. H.; Wang, P.; Palermo, R. X-ray structure of a novel matrix metalloproteinase inhibitor complexed to stromelysin. *Protein Sci.* **2001**, *10*, 923−926.

(89) Wada, C. K.; Holmes, J. H.; Curtin, M. L.; Dai, Y.; Florjanic, A. S.; Garland, R. B.; Guo, Y.; Heyman, H. R.; Stacey, J. R.; Steinmn, D. H.; Albert, D. H.; Bouska, J. J.; Elmore, I. N.; Goodfellow, C. L.; Marcotte, P. A.; Tapang, P.; Morgan, D. W.; Michaelides, M. R.; Davidsen, S. K. Phenoxyphenyl sulfone *N*-formylhydroxylamines (retrohydroxamates) as potent, selective, orally bioavailable matrix metalloproteinase inhibitors. *J. Med. Chem.* **2002**, *45*, 219−232.

(90) Robinson, R. P.; Laird, E. R.; Donahue, K. M.; Lopresti-Morrow, L. L.; Mitchell, P. G.; Reese, M. R.; Reeves, L. M.; Rouch, A. I.; Stam, E. J.; Yocum, S. A. Design and synthesis of 2-oxo-imidazolidine-4-carboxylic acid hydroxamides as potent matrix metalloproteinase-13 inhibitors. *Bioorg. Med. Chem. Lett.* **2001**, *11*, 1211−1213.

(91) Engel, C. K.; Pirard, B.; Schimanski, S.; Kirsch, R.; Habermann, J.; Klingler, O.; Schlotte, V.; Weithmann, K. U.; Wendt, K. U. Structural basis for highly selective inhibition of MMP-13. *Chem. Biol.* **2005**, *12*, 181−189.

(92) *SYBYL Molecular Modeling Package*, version. 6.6; Tripos, St. Louis, MO, 1999.

(93) (a) Halgren, T. Maximally diagonal force constants in dependent angle-bending coordinates. II. Implications for the design of empirical force fields. *J. Am. Chem. Soc.* **1990**, *112*, 4710−4723. (b) Halgren, T. MMFF VI. MMFF94s option for energy minimization studies. *J. Comput. Chem.* **1999**, *20*, 720−729.

(94) Relibase+, version 1., available from Cambridge Crystallographic Data Center (http://www.ccdc.cam.ac.uk/).

(95) Web site at Wayne State University, Detroit, MI: http://sun2.science.wayne.edu/∼somgroup.

(96) *MOE*, version 2001.01, available from Chemical Computing Group, Inc. (http://www.chemcomp.com/).

(97) Dhanaraj, V.; Williams, M. G.; Ye, Q.-Z.; Molina, F.; Johnson, L. L.; Ortwine, D. F.; Pavlovsky, A.; Rubin, J. R.; Skeean, R. W.; White, A. D.; Humblet, C.; Hupe, D. J.; Blundell, T. L. X-ray structure of gelatinase A catalytic domain complexed with a hydroxamate inhibitor. *Croat. Chem. Acta* **1999**, *72*, 575−591.

(98) Jacobson, M.; Sali, A. Comparative protein structure modeling and its applications to drug discovery. *Annu. Rep. Med. Chem.* **2004**, *39*, 259−276.

(99) (a) Blundell, T. L.; Carney, D. P.; Gardner, S.; Hayes, F. R. F.; Howlin, B.; Hubbard, T. J. P.; Overington, J. P.; Singh, D. A.; Sibanda, B. L.; Sutcliffe, M. J. Knowledge-based protein modeling and design. *Eur. J. Biochem.* **1988**, *172*, 513−520. (b) Sutcliffe, M. J.; Haneef, I.; Carney, D. P.; Blundell, T. L. Knowledge-based modeling of homologous proteins. Part I: three-dimensional frameworks derived from the simultaneous superposition of multiple structures. *Protein Eng.* **1987**, *1*, 377−384. (c) Sutcliffe, M. J.; Hayes, F. R. F.; Blundell, T. L. Knowledge based modeling of homologous proteins. Part II: Rules for the conformations of substituted side chains. *Protein Eng.* **1987**, *1*, 385−392.

(100) Baroni, M.; Costantino, G.; Cruciani, G.; Riganelli, D.; Valigi, R.; Clementi, S. Generating optimal linear PLS estimations (GOLPE): an advanced chemometric tool for handling 3D-QSAR problems. *Quantum Struct.−Act. Relat.* **1993**, *12*, 9−20.

(101) McMartin, C.; Bohacek, R. S. QXP: powerful, rapid computer algorithms for structure-based drug design. *J. Comput.-Aided Mol. Des.* **1997**, *11*, 333−344.